sustainability

MDPI

Article

Sustainable Strategies for Removing Advanced Oxidation Byproducts via Microbial Degradation During Petroleum Hydrocarbon Remediation

Shuhai Sun [1,†], Chun Xu [1,†], Xinyu Jiang [1], Jiaxin Yu [1], Wei Fan [2], Zhixing Ren [3,*] and Yu Li [4,*]

[1] School of Hydraulic Engineering, Changchun Institute of Technology, Changchun 130012, China; sh_ssh@ccit.edu.cn (S.S.); 20231061225@stu.ccit.edu.cn (C.X.); 20241371227@stu.ccit.edu.cn (X.J.); yujiaxin@stu.ccit.edu.cn (J.Y.)
[2] Baicheng City Yinnen to Baicheng Project Construction Management Bureau, Baicheng 137319, China; fanwei0005@outlook.com
[3] College of Jilin Emergency Management, Changchun Institute of Technology, Changchun 130021, China
[4] College of Environment and Engineering, North China Electric Power University, Beijing 102206, China
* Correspondence: renzhixingryy@outlook.com (Z.R.); liyuxx8@hotmail.com (Y.L.)
† These authors contributed equally to this work.

Abstract

Using density functional theory (DFT) and the Gaussian 09 program, the study calculated Gibbs free energy to understand how easily each NP can transform. Results showed that only 2,6-dinitrophenol (2,6-DNP) and 2-chloro-6-nitrophenol (2-Cl-6-NP) had Gibbs free energies above 0 kJ/mol. The study also evaluated the toxicity of the NPs, leading to the identification of trinitrophenol (TNP), 2-chloro-4-nitrophenol (2-Cl-4-NP), and 2-nitrophenol (2-NP) with the highest risk scores. In the present study, binding energies were used only as comparative indicators of enzyme–substrate interaction favorability within a screening framework, rather than direct measures of catalytic degradation efficiency. The enzyme 1,2-dioxygenase from Acinetobacter baylyi ADP1 showed strong degradation effects on catechol, with significant binding energies for 2-NP, 2-Cl-4-NP, and TNP. The PS-AOP changed the degradation environment, which reduced enzymatic efficiency. The study also modified specific amino acids in enzymes to improve their performance. For example, the enzyme 1DLT-6 had a degradation increase of nearly 27% compared to the reference enzyme. Finally, we tried to measure the impact of different forces on the breakdown of nitrophenols by enzymes. We used a two-dimensional amino acid map based on enzyme–ligand interactions and a visualization of non-covalent interactions. Our findings show that van der Waals forces and electrostatic forces are the main factors affecting how well the material breaks down. From a sustainability perspective, the study highlights a promising strategy for mitigating secondary pollution, improving the environmental compatibility of PS-AOP-based remediation, and supporting safer and more sustainable restoration of petroleum hydrocarbon-contaminated soil and groundwater. These findings help strengthen the theoretical basis for developing greener post-oxidation remediation pathways.

Keywords: nitrophenols; microbial degradation; sustainable remediation; secondary pollution control; contaminated site restoration; molecular dynamics simulation

Academic Editor: Rosa Rodriguez

Received: 23 February 2026
Revised: 7 April 2026
Accepted: 8 April 2026
Published: 11 April 2026

1. Introduction

The PS-AOP process, which is principally reliant upon sodium persulfate ($Na_2S_2O_8$), is frequently utilized in the remediation of petroleum hydrocarbon-contaminated sites [1,2]. However, this assertion fails to acknowledge the fact that $Na_2S_2O_8$ dissociates into persulfate ions ($S_2O_8^{2-}$) in aqueous solutions, which are relatively stable oxidizing agents [1,3]. Upon activation, $S_2O_8^{2-}$ decomposes into highly reactive sulfate radicals ($SO_4^{2-}\cdot$) and hydroxyl radicals (-OH), which react with naturally occurring NO_2^- in soil and groundwater to form a moderate oxidant—nitrogen dioxide radicals ($NO_2\cdot$) [4,5]. $NO_2\cdot$ has been observed to react with residual phenolic compounds (e.g., phenol, chlorophenols) in petroleum-contaminated sites through hydrogen abstraction, electrophilic addition, or substitution reactions, subsequently generating nitration byproducts (NPs) [6,7]. NO_2^- is an anion found in atmospheric aerosols, surface water, groundwater, and soil, with higher concentrations found in anoxic groundwater [8]. Consequently, when implementing PS-AOP for the degradation of petroleum hydrocarbons in soil and groundwater, the potential for NO_2^- to generate byproducts should be taken into account. Ji et al. [9] initially reported that in the presence of NO_2^- and under the action of SO_4^{2-}, phenol (PhOH) oxidizes to form various NPs, including 2-NP and p-nitrophenol (PNP). Quantum mechanical calculations by Bedini et al. [10] indicated that the reaction between phenoxy radicals and $NO_2\cdot$, catalyzed by water molecules, produces 2,4-DNP, 2,6-DNP, and TNP through hydrogen rearrangement. Yuefei Ji, Lu Wang et al. [11] also demonstrated that NPs are oxidized by SO_4^{2-} to form a key intermediate (phenoxy radical). This intermediate undergoes further transformation through autocatalysis and/or reaction with NO_2^-, leading to the formation of various polynitrophenols. The findings, when considered collectively, provide substantial evidence that NPs are indeed being generated. Furthermore, NPs are archetypal persistent organic pollutants, exhibiting a high degree of resistance to degradation. 2,4-DNP exposure has been demonstrated to induce symptoms such as hypertonia, acidosis, and tachycardia in humans [12]. Nitrophenols, particularly polynitrophenols, have been demonstrated to exhibit toxicity and mutagenicity [13]. Of these, PNP has been shown to possess carcinogenic, teratogenic, and mutagenic properties, leading to its designation as a Priority Contaminant by the U.S. Environmental Protection Agency [14]. This underscores the necessity of addressing the drawbacks of the PS-AOP process and filling gaps in its subsequent application. The present study employs microbial degradation methods to degrade NPs in soil and groundwater. The approaches of physical and chemical degradation were excluded due to the inherent advantages of microbial degradation. The advantages of microbial degradation include the avoidance of difficulties associated with physical degradation, such as soil disturbance or non-recoverable residual adsorbents [15–17]. Additionally, microbial degradation reduces the risks of altered physicochemical properties in soil and water caused by chemical degradation [18]. The process of microbial degradation is chiefly dependent on the secretion of degradative enzymes by microorganisms, which facilitate the absorption, metabolism, and degradation of NPs. This process is characterized by its ability to minimize disturbance, reduce secondary pollution, and maintain low operational costs, thereby ensuring a low risk profile. A plethora of international studies have previously documented the degradation capabilities of various microorganisms. For instance, Hofrichter et al. demonstrated that the *Penicillium* sp. strain Bi7/2 can degrade three types of NPs [19]. Furthermore, the degradation potential of *Bacillus* sp. MW-1 [20], Bacillus subtilis RKJ 700 [21], and *Pseudomonas* sp. JHN [22] has been indicated. However, there is a paucity of studies that have quantitatively assessed degradation efficacy from the perspective of degradative enzymes in post-PS-AOP-treated environments. To the best of our knowledge, no research has employed amino acid sequence modification to enhance enzyme degradation of NPs, nor have many explored the mechanisms of microbial NP

degradation from an enzymatic perspective. Importantly, from a sustainability perspective, remediation strategies should not only remove primary petroleum hydrocarbon pollutants but also minimize secondary pollution, ecological disturbance, and additional chemical burdens to soil and groundwater systems. Therefore, developing biologically compatible post-treatment strategies for PS-AOP byproducts is essential for improving the overall environmental sustainability of contaminated-site remediation.

This study investigates the role of nitrophenols (NPs) as the primary secondary pollutants. The Gaussian 09 program has been instrumental in elucidating the role of Gibbs free energy in DFT calculations as a pivotal indicator for chemical reactions, thereby determining the ease with which NPs undergo transformation pathways. The TOPKAT module, a component of toxicokinetic modeling, is employed to predict the mutagenicity, carcinogenicity, and potential developmental toxicity of NPs. Integrating Gibbs free energy results with toxicity predictions, the Weighted Sum of Moments (WSM) method quantifies and ranks NPs' hazards. Subsequently, molecular docking between target molecules and identified enzymes yields complex information for molecular dynamics simulations. In the present study, binding energies were used only as comparative indicators of enzyme–substrate interaction favorability within a screening framework, rather than direct measures of catalytic degradation efficiency. Mechanisms for varying degradation rates are analyzed through non-bonding interactions and intermolecular energy perspectives. This study provides a theoretical basis for identifying priority secondary pollutants and screening potential degradative enzymes for PS-AOP-treated environments. Beyond mechanistic insight, the work contributes to sustainable remediation by supporting strategies that can reduce secondary contamination risks, improve the environmental compatibility of oxidation-based treatment, and promote safer restoration of petroleum hydrocarbon-contaminated soil and groundwater.

2. Materials and Methods

2.1. Obtaining the Structures of NPs and Their Degrading Enzymes—PDB, UniProt and PubChem Database

Enzymes effectively degrade organic contaminants. Various enzymes, including oxygenases, reductases, hydroxylases, dehydrogenases, and hydrolases, can break down NPs. For instance, the oxygenase PnpA1 from the PNP2-monooxygenase system of the Gram-positive Rhodococcus strain RKJ300 enables denitrification and dichlorination by interacting with different sites on NPs, producing various alcohols [17,18]. Zhang et al. [19] found that the p-benzoquinone reductase PnpB in the Pseudomonas strain WBC-3 is crucial for degrading p-nitrophenol (PNP). Suresh B. Pakala [20] first identified PNP hydroxylase components in Gram-negative Serratia strains. Additionally, studies show that 2,6-dichloro-4-nitrophenol (DCNP) inhibits the activity of alcohol and aldehyde dehydrogenases [21]. Therefore, in this paper, eight monooxygenases were found: membrane-integrated methane monooxygenase of Methylomicrobium alcaliphilum 20Z (PDB ID: 6CXH) [22], single-component monooxygenase of *Burkholderia* sp. strain SJ98 (UniProt ID: J9QWG2) [23], flavin-dependent monooxygenase of Cellvibrio sp. BR (PDB ID: 4USQ) [24], PCP-4-monooxygenase of Sphinomonas sp. UG30 (UniProt ID: O68978) [25], chlorophenol 4-monooxygenase of *Burkholderia cepacia* AC1100 (PDB ID: 3HWC) [26], Streptomyces avermitilis cytochrome P450 enzyme (PDB ID: 3E5K) [27], *Burkholderia* sp. Strain DNT 4-methyl-5-nitrocatechol oxygenase (UniProt ID: Q2PWU9) [28], Geobacillus thermodenitrificans long-chain alkane monooxygenase (PDB ID: 3B9N) [29]; 5 hydroxylases were found: Methylococcus capsulatus methane monooxygenase (PDB ID: 1FZI) [30], Methylosinus sporium methane monooxygenase (PDB ID: 6D7K) [31], *Arcobacter* sp. (UniProt ID: A0A2D5P5B1) [32], Methyllosinus trichosporium methane monooxygenase hydroxylase

(PDB ID: 1MHZ) [33], Methyllosinus trichosporium methane monooxygenase hydroxylase (PDB ID: 6VK6) [34]; 3 dehydrogenases were found: Pseudomonas aeruginosa aldehyde dehydrogenase (PDB ID: 4CAZ) [35], Staphylococcus aureus aldehyde dehydrogenase (PDB ID: 6K10) [36], Saccharomyces cerevisiae alcohol dehydrogenase (PDB ID: 1Q1N) [37]; 7 dioxygenases were found: procatechic acid 2,3-dioxygenase of *Brevibacterium fuscum* (PDB ID: 2IGA) [38], 1,2-Dioxygenase of Hydroxychinol in Pseudomonas cepacia (UniProt ID: A0A2S8I652) [39], Acinetobacter baylyi ADP1 catechol 1,2-dioxygenase (PDB ID: 1DLT) [40], Catechol 1,2-dioxygenase from Pseudomonas putida (PDB ID: 2AZQ) [41], Achromobacter xylosoxidans 2,3-dioxygenase (UniProt ID: D2XKL2) [42], Pseudomonas alkylphenolica 2,3-dioxygenase (PDB ID: 3HPY) [43], Acinetobacter radioestens OB3b catechol 1,2-dioxygenase (PDB ID: 2XSR) [44]; and various hydrolase and reductases were found: epoxide hydrolase of Aspergillus niger (PDB ID: 3G02) [45], epoxide hydrolase of Rhodococcus erythropolis (PDB ID: 4XBT) [46], epoxide hydrolase of Bacillus megaterium (PDB ID: 4IO0) [47], p-benzoquinone reductase of Pseudomonas putida WBC-3 (PDB ID: 4LA4) [19]. After the PS-AOP process, phenol (PhOH) that isn't fully degraded can be oxidized by nitrogen dioxide ($NO_2\cdot$), leading to the formation of NPs, particularly 2-nitrophenol (2-NP) and paranitrophenol (PNP). Further oxidation can produce compounds such as binitrophenol, chloronitrophenol, and trinitrophenol. The key pollutants to be studied are 2-NP, PNP, 2,4-dinitrophenol (2,4-DNP), 2,6-dinitrophenol (2,6-DNP), trinitrophenol (TNP), 2-chloro-4-nitrophenol (2-Cl-4-NP), 2-chloro-6-nitrophenol (2-Cl-6-NP), and 2-chloro-4,6-dinitrophenol (2-Cl-4,6-DNP). Enzyme structures were obtained from the Protein Data Bank (PDB, www.rcsb.org) and the UniProt protein structure database (www.uniprot.org), while the molecular structures of the compounds were sourced from the organic small molecule biological activity database (PubChem, https://www.pubchem.ncbi.nlm.nih.gov).

2.2. Assessing the Ease of Translating NPs—Gibbs Free Energy Calculation

Density functional theory (DFT) is a method for calculating the properties of solid materials based on electron density. A key concept in DFT is Gibbs free energy (G), which indicates the stability of a substance at specific temperatures and pressures. Gibbs free energy, expressed in kJ/mol, is defined as the difference between enthalpy and the product of temperature and entropy. Under isothermal and isobaric conditions, changes in Gibbs free energy determine the spontaneity of reactions, making it crucial in pharmaceutical science [48]. In DFT, Gibbs free energy is calculated from the internal energy, volume, and entropy of the system at various conditions [49]. It is essential for analyzing chemical reaction equilibria and characterizing a compound's reactivity [50]. This paper uses density functional theory (DFT) to optimize molecules at the B3LYP/6-31G(d) basis set level with the Gaussian 09 program. It calculates the Gibbs free energy of the molecules to assess the difficulty of different nitrophenol conversion pathways. The calculation formula is as follows:

$$\Delta G = \sum G(\text{products}) - \sum G(\text{reagent}) \quad (1)$$

where $\sum G$ (products) represents the Gibbs free energy of the various nitrophenol products in the conversion pathway, and $\sum G$ (reagent) represents the Gibbs free energy of the various nitrophenol reactants in the conversion pathway. Firstly, Gauss View 5.0 software should be utilised to create a TOP file for the reactants and products, with the parameters being specified. Thereafter, a molecular dynamics simulation should be performed by setting an array of λ-point values.

Note: PS-AOP nitration/oxidation proceeds via radical pathways and is often kinetically controlled. In this study, ΔG is used only as a screening-level thermodynamic descriptor for pathway plausibility; activation barriers (ΔG‡) and rate constants were not computed, which limits any quantitative inference regarding product yields.

2.3. Predicting the Toxicity of NPs—Toxicokinetic Modeling (TOPKAT)

The Food and Drug Administration (FDA) and the National Toxicology Program (NTP) provide a comprehensive rodent carcinogenicity module as part of the TOPKAT (Developed by the American company Accelrys) package within the Discovery Studio 2020 software. This module features statistically robust and cross-validated Quantitative Structure–Activity Relationship (QSAR) models that are instrumental in assessing the toxicity of a wide range of chemical compounds [51]. In the realm of drug development, toxicology research holds a critical position, guiding the safety and efficacy of new therapeutic candidates. By leveraging predictive models to evaluate the potential health risks these candidate compounds pose to humans, we aim to identify and eliminate those with concerning safety profiles early in the research process. This proactive approach enables us to focus on selecting the most promising compounds for in-depth screening and biological testing. Ultimately, this strategy is designed to minimize both research costs and the inherent risks associated with drug development [52,53]. This study employs the TOPKAT module in Discovery Studio 2020 software to predict mutagenicity, skin sensitization, skin irritancy, ocular irritancy, and rodent carcinogenicity of NPs compounds, assessing the associated human health risks [54,55].

2.4. Quantifying the Comprehensive Toxicity of Nitrophenols—Weighted Scoring Method

The weighted scoring method is a widely used evaluation technique that assigns weights to each factor based on its importance and scores them accordingly. The total score is calculated through a weighted sum, allowing for a quantifiable assessment of multiple factors' impacts on the target variable. This method is particularly effective for evaluating parallel factors. For example, Wang et al. created a weighted scoring model to annotate and prioritize non-coding variants related to their functions [56]. This method integrates thermodynamic plausibility and predicted toxicity endpoints to generate a screening-level prioritization score for nitrophenols, intended to guide follow-up assessment rather than serve as a validated quantitative risk model. Prior to weighting, each criterion is normalized to [0, 1] across the eight NPs (min–max scaling). The final score is computed as $S_i = \sum_j w_j x_{ij}$, where w_j denotes the criterion weight and x_{ij} the normalized value of criterion j for compound i. For TOPKAT endpoints, probability values are directly used; for ΔG, the mapped thermodynamic descriptor is normalized consistently. The calculation formula is as follows:

$$S_{A,B} = W_i + s_i \quad (2)$$

$$\sum S = S_1 + S_2 \quad (3)$$

In the formula, i represents nitrophenyl compounds, assigned values from 1 to 8 based on the following: 2-NP, PNP, 2,4-DNP, 2,6-DNP, TNP, 2-Cl-PNP, 2-Cl-6-NP, and 2-Cl-4,6-DNP. W is the weight, s is the score, S is the weighted score, and the weighted total score is $\sum S$. We performed a sensitivity analysis by varying the thermodynamic vs toxicity weight split (e.g., 30/70 to 70/30) and examining whether the top-ranked NPs remain unchanged.

2.5. Quantifying the Enzymatic Degradation of Nitrophenols—Molecular Dynamics Simulation

2.5.1. Molecular Docking

The process begins with the selection of Discovery Studio 4.0 software, developed by Biovia, for molecular docking analysis. The first step involves importing the receptor protein crystal structure and performing several preprocessing tasks, such as removing water molecules, metal ions, and any existing ligand molecules to ensure a clean structure. Once the protein is prepared, the LibDock module is employed to designate the protein as the receptor molecule for docking studies. Next, the "Find Sites from Receptor Cavities"

function within the Define module is utilized to identify potential binding sites within the receptor protein. After the binding sites are located, modifications are made to refine their characteristics, ensuring optimal suitability for ligand docking. Finally, the ligand molecules are integrated into the defined binding cavities of the protein, positioning them to facilitate an effective docking interaction for further analysis and evaluation.

2.5.2. Molecular Dynamics Simulation

Molecular dynamics, a molecular simulation method based on Newtonian mechanics, provides information on protein thermodynamics, kinetics, and other macroscopic properties. Its extensive application in the domains of chemical and pharmaceutical research is attributable to its efficacy in the analysis of intermolecular interactions. It is commonly used in chemistry and drug research to analyze intermolecular interactions. The Dell PowerEdge R7425 server was used with GROMACS 5.1.4 software (released by the team from the University of Groningen in The Netherlands) to analyze a system of nitrophenol (NP) molecules and target protein molecules in a periodic dodecacuum of 15 nm [57]. The GROMOS96 43a1 force field facilitated molecular constraints, and Na^+ ions were added for charge neutralization. The molecular dynamics simulation has four main steps. The simulation begins with an energy minimization step, using the fastest descent method to reduce energy levels until they converge at 1000 kJ/mol, which signifies that the system has reached an equilibrium state. Following this, the temperature is carefully controlled at 300 K within both a macroscopic regular ensemble and an isothermal isopressurized ensemble, while maintaining a pressure of 1 bar to ensure the stability of the ligand–protein complex. Once these conditions are established, the simulation enters the equilibrium phase: position constraints are released, allowing for greater freedom of movement, and the leapfrog Newton's integration method is implemented with a time step of 2 fs. This process unfolds over a total duration of 1 ns, encompassing 500,000 steps at the set temperature and pressure, enabling an in-depth exploration of the molecular interactions involved [58,59]. The 1 ns MD simulations performed in this study were intended as preliminary conformational sampling for comparative screening. We acknowledge that this timescale is insufficient to demonstrate full equilibration or rigorous convergence for enzyme–ligand systems, and therefore the resulting MM-PBSA energies should be interpreted cautiously. The free energy calculation formula is combined as follows (3)–(5) [60,61]. The binding energy of NPs molecules in solution to degrading enzymes:

$$Gbind = Gcomplex - Gfree - protein - Gfree - ligand \quad (4)$$

$$G = Egas - TSgas + Gsolvation \quad (5)$$

$$Gsolvation = Gpolar + Gnonpolar \quad (6)$$

To predict how effectively bacteria degrade NPs, we start by removing water, hydrogenating, and modifying the charge of the receptor protease to define the protein's binding cavity. We select target molecules—2-NP, PNP, 2,4-DNP, 2,6-DNP, TNP, 2-Cl-4-NP, 2-Cl-6-NP, and 2-Cl-4,6-DNP—as ligands, along with eight secondary pollutants, and load them into the Discovery Studio 2020 software. Using molecular dynamics, a simulation method based on Newtonian mechanics, we analyze protein thermodynamics and dynamics to study intermolecular interactions. Finally, we calculate the binding energy between various enzymes and NPs and use these values as comparative descriptors of enzyme–substrate interaction favorability for preliminary screening of potential biodegradation compatibility, rather than as direct measurements of catalytic degradation efficiency. (Because the present MM-PBSA analysis was performed on short MD trajectories for comparative screening purposes, statistical uncertainty estimates were not used as the basis for

ranking in this study. Future work will incorporate longer simulations and replicate-based uncertainty analysis.)

2.6. Optimized Design of 1,2-Dihydroxybenzene Dioxygenase—Homologous Modeling Method

Homology modeling is a method used to create a model of an unknown protein structure by using a related protein with a known structure as a template. In this study, the amino acid sequence of catechol 1,2-dioxygenase (PDB ID: 1DLT) from Acinetobacter baylyi ADP1 was obtained from NCBI. Using Discovery Studio 4.0, we performed molecular docking to identify key amino acid residues within the enzyme's active site that interact with selected natural products (NPs). Once we pinpointed these critical residues, we rationally substituted them to develop new amino acid sequences. We then submitted these modified sequences to SWISS-MODEL at the Glaxo Smith Kline Center in Geneva, Switzerland, with the goal of generating a new structural model of the enzyme employing the homologous modeling approach. This comprehensive process allowed us to explore potential enhancements in the enzyme's structure and function. The structural rationality of the built model was assessed using the Ramachandran conformation map from the SAVES server at UCLA-DOE. This map includes an optimal region (red), a sub-permitted region (yellow), a general allowable region (light yellow), and a non-permitted region (white). If the combined percentages of the optimal, sub-permitted, and general permissible regions exceed 95%, the constructed protein and enzyme are considered reliable. The redesign strategy adopted here was intended as a rational, interaction-guided computational exploration of potentially improved variants. It does not constitute a direct mechanistic proof of catalytic enhancement. The redesign strategy adopted here was intended as a rational, interaction-guided computational exploration of potentially improved variants. It does not constitute a direct mechanistic proof of catalytic enhancement.

3. Results and Discussion

3.1. Derivation of Conversion Pathways for Various Nitrophenols in the PS-AOP Process

According to the findings of the studies conducted in this field, the presence of SO_4^{2-}, which is produced by the decomposition of activated $S_2O_8^{2-}$, has been demonstrated to play a crucial role in the oxidation of PhOH. However, it has been observed that PhOH exhibits a high degree of stability in the presence of NO_2^- or NO_3^- alone, suggesting that the presence of these anions does not significantly affect the oxidation process [9]. This happens when $SO_4^{-}\cdot$ reacts with NO_2^-, producing $NO_2\cdot$, which can oxidize electron-rich compounds like phenol, aniline, and ascorbates. The reaction rate ranges from 106 to 108 $M^{-1}s^{-1}$ [55]. $NO_2\cdot$ initiates the reaction by capturing hydrogen from phenol, forming HNO_2 and a phenoxy radical [62]. The phenoxy radical then reacts with another $NO_2\cdot$ to create nitrophenol. Polynitrophene is formed from mononitrophenes, and $SO_4^{-}\cdot$ can generate free radical cations through electron transfer [8]. The formation pathway of nitrophenol is shown in Figures 1 and 2.

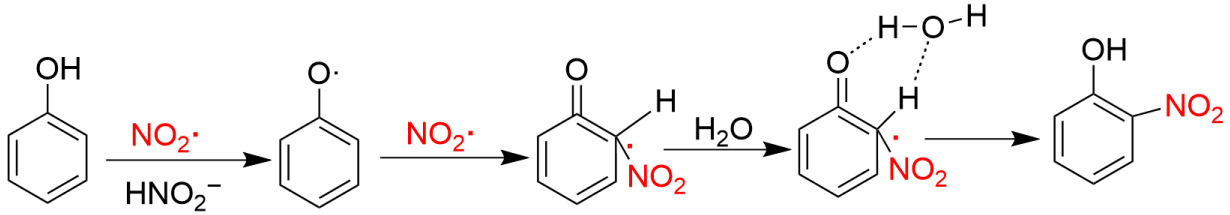

Figure 1. Proposed conversion pathways of mononitrophenols during the PS-AOP oxidation process.

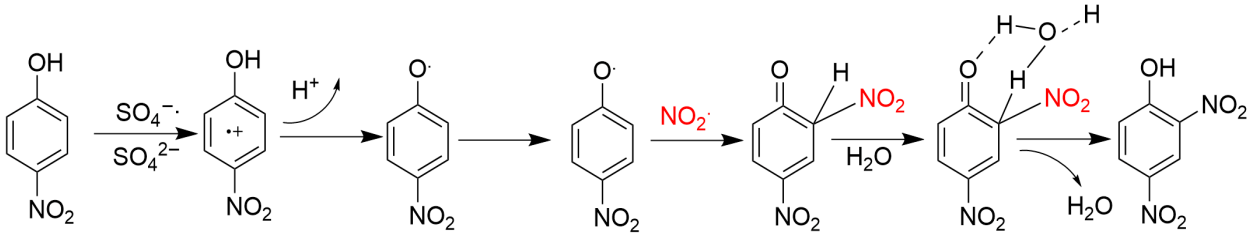

Figure 2. Conversion Pathways of Polynitrophenol during the PS-AOP Oxidation Process. Note: Arrows indicate hypothesized transformation directions inferred from literature evidence and thermodynamic screening.

In light of the synthesis pathways of 2-NP and 2,4-DNP (as illustrated in Figures 1 and 2) and the aforementioned analysis, the formation mechanisms of other products are deduced as illustrated in Figure 3.

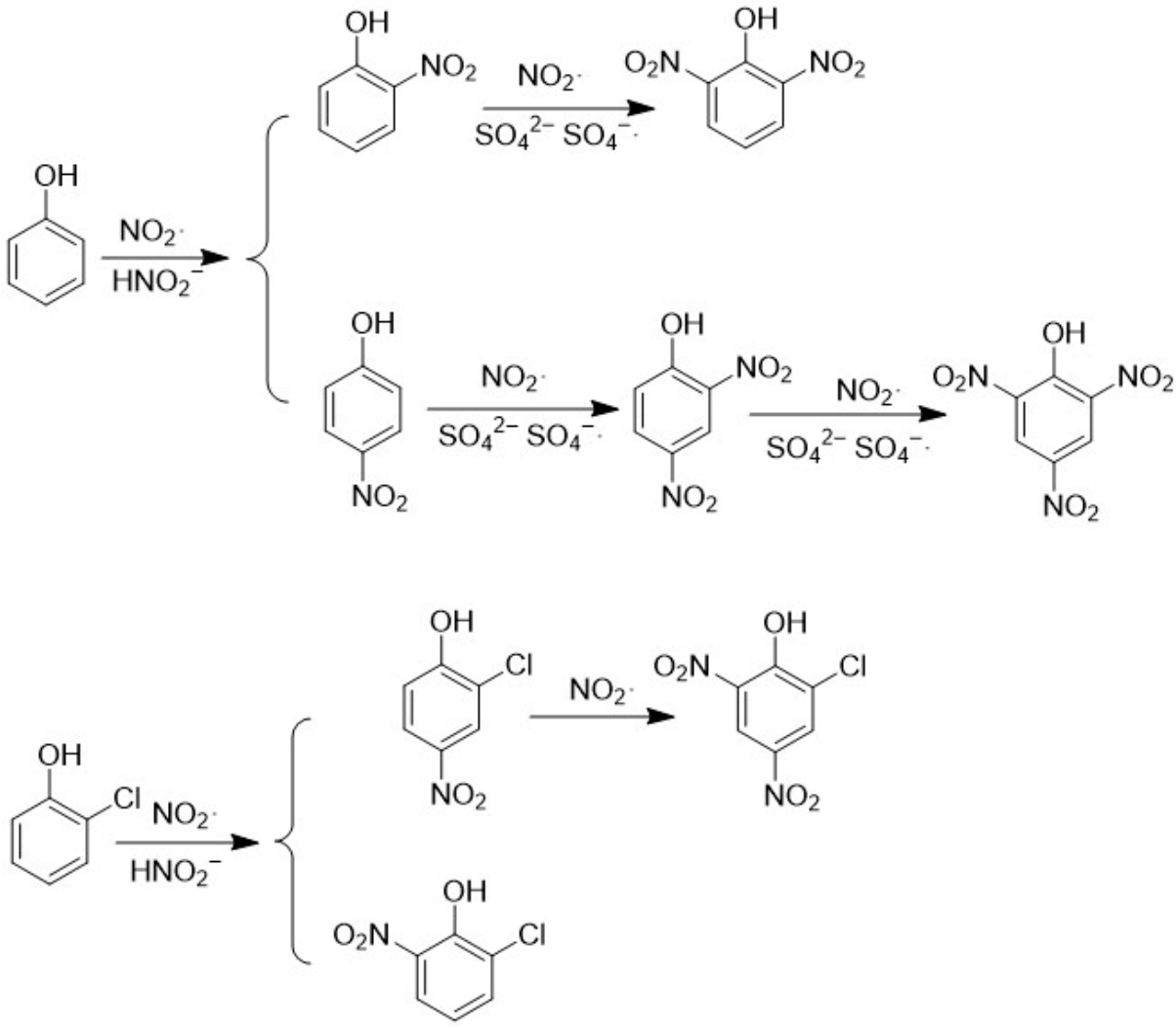

Figure 3. Alternative Conversion Pathways of Other Nitrophenols During Oxidation.

Gibbs free energy functions as a criterion for evaluating the ease of reaction occurrence and can explain the direction of spontaneous chemical reactions [62]. Gibbs free energies were found to be less than 0 kJ/mol, indicating that these reactions proceed spontaneously under SO_4^{2-} mediation. A Gibbs free energy greater than 0 kJ/mol signifies that the reaction necessitates energy from the external environment [56]. The DFT calculations were performed using Gaussian 09, and the resulting Gibbs free energies are

summarized in Table 1. Preliminary research suggests that the formation of 2,4-dihydroxy-N-nitroso-benzene (2,4-DNP) and 2-chloro-4-nitro-benzene (2-Cl-4-NP) is twice that of 2,6-dihydroxy-N-nitroso-benzene (2,6-DNP) and 2-chloro-6-nitro-benzene (2-Cl-6-NP). As demonstrated in Table 1, the Gibbs free energies for both 2,4-DNP and 2-Cl-4-NP are less than 0 kJ/mol, suggesting that these pathways are thermodynamically more plausible under the adopted assumptions; however, no direct inference about actual product yields can be made without kinetic analysis. The calculated ΔG values support the thermodynamic plausibility of the proposed transformation pathways under the stated computational assumptions. However, product yields in PS-AOP radical systems are governed by kinetic competition and activation barriers (ΔG‡); therefore, ΔG should not be interpreted as a predictor of formation yield without transition-state/rate-constant analysis. A thorough analysis of the computational results reveals that 2-NP, PNP, 2,4-DNP, TNP, 2-Cl-4-NP, and 2-Cl-4,6-NP are more readily formed than 2,6-DNP and 2-Cl-6-NP.

Table 1. Calculation Results of NPs Gibbs Free Energy.

Reactant	Product	Gibbs Free Energy (kJ/mol)
PhOH	2-NP	−0.001126
PhOH	PNP	−0.001126
2-NP	2,4-DNP	−0.000204
2-NP	2,6-DNP	0.0006
2,4-DNP	TNP	−0.001065
2-CP	2-Cl-4-NP	−0.001199
2-CP	2-Cl-6-NP	0.000186
2-Cl-4-NP	2-Cl-4,6-DNP	−0.000133

3.2. Prediction of Nitrophenols Toxicity Based on Toxicokinetic Models (TOPKAT)

The TOPKAT system utilizes a probability value ranging from 0 to 1 as the foundation for predicting and assessing toxic effects. This probability value is categorized into three distinct intervals: low probability (0–0.3), uncertain (0.3–0.7), and high probability (0.7–1). Each interval represents a level of risk associated with potential toxicity. Specifically, a lower probability indicates a minimal risk of toxic effects, while higher values suggest a greater likelihood of toxicity. In addition to categorizing risk, TOPKAT can also predict specific toxicity levels and evaluate the potential impacts based on the assigned probability range. A higher probability value, alongside an elevated toxicity level, signifies an increased risk of adverse health effects and indicates that the substance in question may pose a greater threat to human health. This section focuses on predicting the behavior and effects of NPs by utilizing a variety of biological models. Specifically, it incorporates biological mutagenicity models, NTP carcinogenicity models, and models designed to assess skin irritation, skin sensitization, and eye irritation. Each of these models is systematically categorized and assigned specific identifiers: D1 for biological mutagenicity, D2 for NTP carcinogenicity, D3 for skin irritation, D4 for skin sensitization, and D5 for eye irritation. For instance, the biological mutagenicity model for 2-NP is designated as 2-NP-D1, indicating its specific application within this comprehensive framework. This structured approach allows for a clearer understanding of the potential risks associated with NPs across different biological contexts.

The prediction results of the TOPKAT model indicators are shown in Figure 4. In the biological mutagenicity model, all NPs, except for 2-Cl-6-NP, present a high probability risk for mutagenicity. NPs and their biotransformation products can cause mutations through nucleotide mismatches during DNA synthesis, resulting in DNA damage [63]. This damage can lead to oxidative stress in the liver of mature male zebrafish, triggering tumor suppressor factor upregulation, increased DNA damage, and activation of apoptosis-related

genes [64]. Additionally, exposure to these NPs can cause the shedding of gill lobule cells and the thinning of gill lobules in loaches. Huang et al. found that all 18 compounds in their chromosome aberration experiments on human lymphocytes were genotoxic [65]. Certain NPs can negatively affect fish embryos and larvae, leading to reduced body length, longer hatching times, yolk sac edema, and abnormal body shapes [66]. In the NTP carcinogenic model, 2-NP, 2,4-DNP, 2,6-NP, TNP and 2-CL-4,6-NP show a high probability risk for adult male mice. PNP is noted for its environmental endocrine-disrupting properties [67], interfering with hormone synthesis and metabolism, which can disrupt testosterone secretion and lead to hormonal imbalances [68,69]. Additionally, PNP undergoes conversion into nitroso and hydroxylamine derivatives within the bodies of humans and mammals. This biochemical transformation can result in the formation of hemoglobin or nitrite amine, both of which are recognized as carcinogens [70]. Research indicates that when PNP enters the human body, it is linked to various serious health issues, including respiratory diseases and an increased risk of lung cancer [62]. In studies assessing skin irritation, all eight types of NP (naphthalene derivatives) displayed a concerningly high probability of causing adverse effects. In the skin sensitization assessment, only 2-NP and PNP were exceptions, as they did not present the same level of risk. Furthermore, the ocular irritation models revealed that all eight NPs were classified as high-risk, exhibiting moderate stimulation to the eyes, which raises significant concerns regarding their safety and potential harm to both health and the environment.

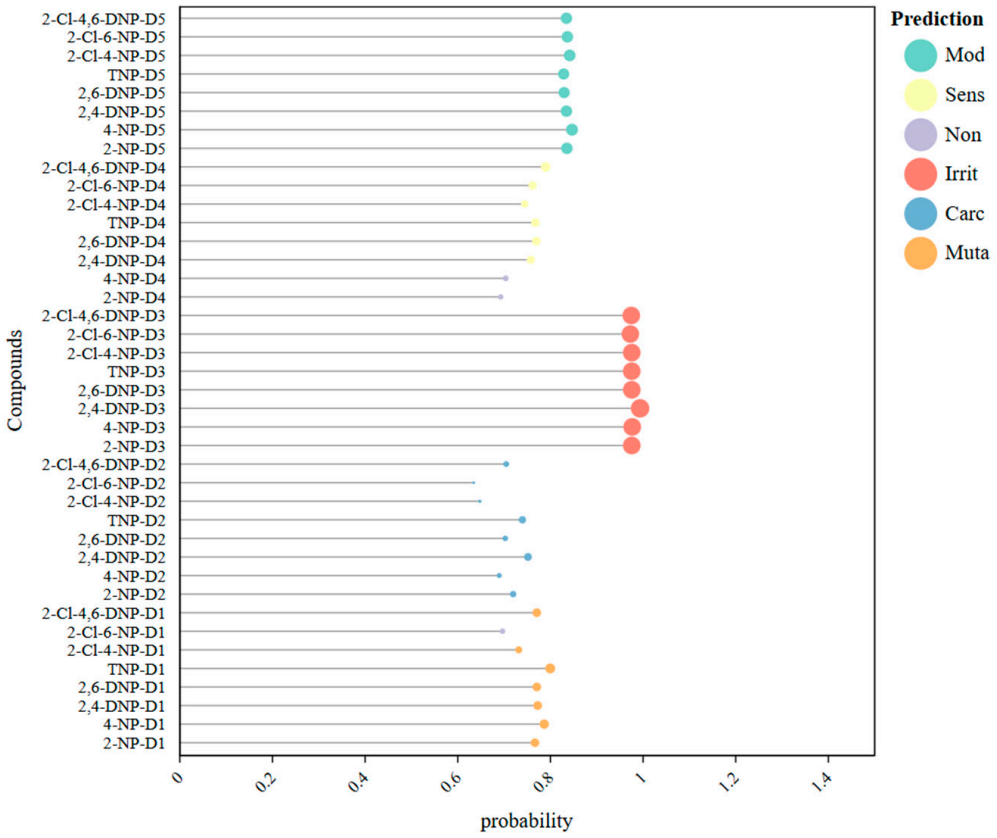

Figure 4. Prediction Results of TOPKAT Model Indicators.

3.3. Comprehensive Toxicity Risk Assessment of Nanomaterials Based on a Weighted Scoring Method

In this study, the weighting scheme was designed to balance two considerations: (i) the thermodynamic plausibility that a compound may be formed during PS-AOP, and (ii) the potential toxicological concern reflected by the predicted toxicity endpoints. There-

fore, Gibbs free energy was assigned a relatively higher weight as a formation-related descriptor, while the five toxicity endpoints were treated equally to reflect their parallel contribution to the overall screening-level hazard profile. We emphasize that this weighting framework is intended for comparative prioritization rather than as a definitive quantitative risk assessment model. Additional sensitivity analysis indicated that moderate variation in the relative thermodynamic/toxicity weighting did not substantially change the identity of the highest-priority compounds, supporting the robustness of the screening outcome.

In this section, the Gibbs free energy and the toxicity prediction probability are considered as factors A and B, respectively. Given the established correlation between Gibbs free energy and both the ease of reaction product formation and, consequently, toxicity severity, the weight (W) assigned to factor A (Gibbs free energy) is set to 0.5. Concurrently, the weights for Ames mutagenicity, NTP carcinogenicity (adult male rats), skin irritation, skin sensitization, and eye irritation are regarded as equivalent. The present study focuses exclusively on toxicity prediction, without delving into the specific hazards associated with different toxicities. Consequently, the weight (W) for all five toxicity prediction factors B is set to 0.1. This scoring method uses a three-tier system (1–3 points). Factor A calculation yields one point if the value is greater than 0 kJ/mol, two points if the value is less than 0 kJ/mol but greater than −0.001 kJ/mol, and three points if the value is less than −0.001 kJ/mol. Factor B is categorized into three probability levels: low probability (0–0.3) receives one point, uncertain probability (0.3–0.7) receives two points, and high probability (0.7–1) receives three points. The total weighted score calculated is shown in Table 2 as follows.

Table 2. Total Risk-Weighted Score for Comprehensive Toxicity of NPs.

Number \ Rating	Gibbs Free Energy Weighted Score (S_A)	Toxicity Prediction Score (S_B)	Weighted Total Score ($\sum S$)
1	1.5	1.1	2.6
2	1.5	1.0	2.5
3	1.0	1.4	2.4
4	0.5	1.4	1.9
5	1.5	1.4	2.9
6	1.5	1.3	2.8
7	0.5	1.2	1.7
8	1.0	1.4	2.4

Based on the final calculations, TNP poses the greatest risk of human exposure among the evaluated molecules, followed by 2-Cl-4-NP. Meanwhile, 2,6-DNP and 2-Cl-6-NP have lower total weighted scores because their degradation pathways are more challenging. This is due to the higher spin density of the unpaired electrons in the para position compared to the ortho position in the phenoxy radical. Therefore, when selecting degrading enzymes, priority should be given to molecules with high toxicity-weighted total scores: TNP, 2-Cl-4-NP, and 2-NP. Subsequent research and discussion in this paper will focus primarily on these three NP categories.

3.4. Comprehensive Effect Evaluation of Microbial Degradation of NPs Based on Molecular Dynamics Simulation

Molecular dynamics simulations were performed using GROMACS version 5.1.4 on a Dell PowerEdge R7425 server on a Dell PowerEdge R7425 server. In the earlier part of this article, two groups of proteins were simulated at a temperature of 300 K and a pressure of 1 bar using the leapfrog Newton integration method with a simulation step size of 2 fs.

The simulation duration was 20 ns, and 10,000,000 simulation steps were conducted. By keeping other variables constant and conducting a simulation with 500,000 simulation steps for 1 ns, the results were compared. The results are shown in the table below.

From the table, it can be seen that the data results of the two are not significantly different. This paper will conduct 216 sets of dynamic calculations. The calculation volume is extremely large, so this paper adopts a 1 ns duration for simulation to save a huge amount of work. This paper once again acknowledges this limitation and clearly states in the text that the molecular dynamics simulation is only carried out as a preliminary screening simulation.

Binding energies between degradative enzymes and NP pollutants across various degradation pathways were calculated to characterize the enzymes' degradation capabilities, as shown in Tables 3 and 4 below.

Table 3. Comparison of Simulation Results at Different Time Intervals.

Compounds Enzymes	1DLT		1FZI	
	20 ns	**1 ns**	**20 ns**	**1 ns**
2-NP	−60.321	−57.022		
2-Cl-4-NP			−23.772	−19.835

Table 4. Calculation Results for the Binding Energy Between Degrading Enzymes and NPs (Unit: kJ/mol).

Enzymes \ Compounds	2-NP	PNP	2,4-DNP	2,6-DNP	TNP	2-Cl-4-NP	2-Cl-6-NP	2-Cl-4,6-DNP
1DLT	−57.022	−53.248	−64.265	−65.343	−69.239	−59.319	−70.044	−66.893
1FZI	−61.645	−46.249	−44.473	−35.548	−30.859	−19.835	−40.292	−19.113
1MHZ	9.287	−51.447	−43.338	−28.082	−8.530	−40.333	−23.857	20.436
1Q1N	−27.571	−43.293	−21.758	−42.157	−44.145	−36.128	−38.092	−43.244
2AZQ	−19.686	0.457	−5.370	−36.541	1.515	−16.272	−41.304	−21.319
2IGA	25.196	2.342	1.937	−17.773	−38.171	−26.605	−11.500	−28.984
2XSR	−9.114	−8.798	−38.287	−31.456	−4.668	−28.303	−15.412	−32.774
3B9N	−26.667	−9.430	−14.212	−13.952	−15.712	−35.107	−43.711	−22.100
3E5K	−23.027	−25.879	−35.553	−30.729	−42.315	−42.216	−12.955	−49.059
3G02	−47.291	−52.611	−5.505	4.079	−7.886	−40.956	−67.354	5.223
3HPY	−32.646	−19.250	−20.399	−13.332	−12.835	−28.749	−43.918	−5.799
4CAZ	−21.209	−40.796	−28.106	−10.456	−44.779	−43.415	−27.016	−16.836
4IO0	−41.282	6.070	−14.679	−37.137	−54.631	−40.758	−40.013	−67.553
4USQ	−38.085	−35.151	−38.943	−29.198	−36.115	−53.438	−34.006	−31.725
4XBT	−49.921	−49.232	−56.896	−61.110	−66.106	−49.420	−35.888	−53.589
6CXH	−23.723	−3.422	−55.351	−33.512	−48.037	−42.541	−19.862	−51.209
6D7K	−33.890	4.469	10.211	−6.428	21.745	−44.145	2.654	14.199
6K10	−49.375	−35.040	−56.225	−47.609	−60.422	−46.047	−41.751	−50.482
6VK6	−18.120	−1.325	1.498	−12.747	−18.122	−52.693	−18.495	−6.049
3HWC	−25.802	−34.935	−41.905	−25.884	−27.971	−30.539	−26.143	−41.240
4LA4	−39.215	−32.360	−44.650	−49.454	−45.375	−45.742	−42.939	−45.778
A0A2D5P5B1	−27.565	−16.608	10.740	−11.183	−17.630	−45.363	−30.699	−27.185
A0A2S8I652	−12.254	−62.712	−30.796	−38.410	−18.912	−45.246	−41.038	−29.352
D2XKL2	−33.917	−38.666	−15.779	−7.037	−18.735	−39.549	−30.888	−11.312
J9QWG2	−27.037	−65.063	−47.551	−44.916	−13.287	−73.420	−47.529	−59.743
O68978	36.568	−30.023	−56.63	−32.691	−38.277	−37.529	−51.888	−38.335
Q2PWU9	−21.010	0.953	8.512	−12.007	−12.912	−12.020	−8.372	−2.535

Among the screened enzymes, catechol 1,2-dioxygenase from Acinetobacter baylyi ADP1 exhibited relatively favorable binding interactions with several high-priority NPs, suggesting that it may be a promising candidate for further mechanistic and experimental evaluation. The monocomponent monooxygenase from *Burkholderia* sp. strain SJ98 demonstrated optimal degradation of PNP, 2,6-DNP, 2-Cl-4-NP, and 2-Cl-4,6-NP. The PCP-4 monooxygenase from Sphingomonas sp. UG30 exhibits relatively stronger interaction with 2,4-DNP and 2-Cl-6-NP. The cytochrome P450 enzyme from Streptomyces avermitilis demonstrates good degradation of TNP, this phenomenon can be attributed to the ability of monooxygenases to more accurately determine the position of the nitro group on the phenyl ring of nitrophenol [17]. These enzymes possess a distinctive "denitration" mechanism, which facilitates the removal of the nitro group with a high degree of precision. During the introduction of a hydroxyl group, the nitro group is concurrently eliminated in the form of $NO_2^{-}\cdot$. Among hydroxylases, the methane monooxygenase hydroxylase from Methylococcus capsulatus showed good degradation of 2-NP, 2,4-DNP, 2,6-DNP, TNP, and 2-Cl-6-NP. Methylosinus trichosporium's methanomonooxygenase hydroxylase more readily degrades PNP. The methanomonoxygenase hydroxylase from Methylosinus trichosporium OB3b exhibits the lowest binding energy with 2-Cl-4-NP, resulting in superior degradation. The hydroxylase from Methylosinus sporium is better suited for degrading 2-Cl-4,6-DNP. Among the various types of dehydrogenase enzymes, Staphylococcus aureus's aldehyde dehydrogenase has been observed to exhibit optimal degradation capabilities against all eight classes of NPs. In contrast, Saccharomyces cerevisiae's alcohol dehydrogenase has demonstrated remarkable effectiveness in the degradation of PNP. Beyond monooxygenases, dioxygenases have also demonstrated considerable potential in the degradation of NP molecules. Acinetobacter baylyi ADP1's 1,2-bisoxygenase for catechol has been identified as a highly efficient NPs degradation enzyme, readily reacting with NPs to achieve degradation. In the context of PNP degradation, Pseudomonas cepacia's 1,2-bisoxygenase for hydroxychinol has been demonstrated to exhibit enhanced efficacy. Hydrolases are enzymes that facilitate the breakdown of macromolecules into smaller fragments. Preliminary calculations of binding energy have indicated generally favorable performance, with epoxide hydrolase from Rhodococcus erythropolis demonstrating strong comprehensive degradation capabilities. The epoxide hydrolase from Aspergillus niger exhibits remarkable efficacy in the degradation of PNP and 2-Cl-6-NP. The p-benzoquinone reductase from Pseudomonas putida WBC-3, a hydrogenase, has been observed to exhibit degradation activity toward all NP molecules. As discussed in Section 3.3, TNP, 2-Cl-PNP, and 2-NP are known for their high overall toxicity. Consequently, the binding favorability of these three compounds should be prioritized when selecting degradative enzymes. The available computational results suggest that catechol 1,2-dioxygenase from Acinetobacter baylyi ADP1 is a promising candidate for further evaluation in NP biodegradation. The enzyme exhibits not only good degradation activity toward all eight NPs but also particularly strong degradation capabilities for TNP, 2-Cl-4-NP, and 2-NP, making it an enzyme with comprehensive degradation potential. Acinetobacter baylyi ADP1, a prominent strain utilized in the study of aromatic compound degradation, exhibits a 1,2-dioxygenase for catechol that functions crucially in the opening of the benzene ring and the initiation of complete degradation. Its robust genetic background and tolerance enable superior survival in toxic NP environments compared to other selected enzymes [71]. The 1,2-dioxygenase of Acinetobacter baylyi ADP1 exhibits strong comprehensive degradation capabilities. Given the limited MD timescale, these results are best interpreted as comparative short-timescale interaction estimates rather than converged free-energy measurements.

3.5. Optimized Design of Novel 1,2-Dioxygenase for Catechol Based on Homologous Modeling

3.5.1. Screening of Novel Dioxygenase Modification Sites in Amino Acid Two-Dimensional Planes

As previously indicated, the 1,2-dioxygenase of Acinetobacter baylyi ADP1 exhibited superior degradation efficacy for various NPs among the selected enzymes. However, the PS-AOP process utilizes acidic solutions, resulting in the presence of residual SO_4^{2-} during the initial contamination site treatment. The processes of cloning and expression of catechol 1,2-dioxygenase are influenced by pH, with an optimal range generally between 7.0 and 9.0 [67]. Acidic conditions have been shown to inhibit its cloning and expression, and enzyme stability is compromised when pH falls below 5.0 [72]. Furthermore, metal ions such as Fe^{3+}, Cu^{2+}, Zn^{2+}, Co^{2+}, Al^{3+}, Cd^{2+}, Ni^{2+}, and Mn^{2+} have been identified as activating metals in PS-AOP processes. These ions have been shown to inhibit dioxygenase activity by 20% to 80% when residual from the activated PS-AOP process [73]. Therefore, this study aims to rationally modify the enzyme by altering its amino acid sequence through homology modeling to further enhance its binding favorability. Using the molecular docking module in Discovery Studio 4.0, the active site amino acids of the 1,2-dihydroxydipheny from Acinetobacter baylyi ADP1 (1DLT) were identified. The active site for 2-NP interaction with 1DLT comprises: 55 (TYR), 58 (GLY), 59 (VAL), 62 (LEU), 71 (ALA), 72 (GLY), 74 (LEU), 75 (SER), 78 (LEU), 80 (PHE). The active site for TNP interaction with 1DLT comprises: 55 (TYR), 58 (GLY), 59 (VAL), 62 (LEU), 71 (ALA), 74 (LEU), 75 (SER), 78 (LEU), 80 (PHE). The active sites for 2,4-DNP interacting with 1DLT are: 55 (TYR), 58 (GLY), 59 (VAL), 62 (LEU), 71 (ALA), 74 (LEU), 75 (SER), 78 (LEU), 80 (PHE). The active sites for 2,4-DNP interacting with 1DLT are: 41 (LEU), 55 (TYR), 58 (GLY), 59 (VAL), 62 (LEU), 71 (ALA), 74 (LEU), 75 (SER), 78 (LEU), 80 (PHE). The active sites for 2,6-DNP interacting with 1DLT are: 55 (TYR), 58 (GLY), 59 (VAL), 62 (LEU), 65 (LEU), 71 (ALA), 74 (LEU), 75 (SER), 78 (LEU), 80 (PHE). The active sites for TNP interacting with 1DLT are: 41 (LEU), 45 (ILE), 50 (ILE), 54 (GLU), 55 (TYR), 58 (GLY), 59 (VAL), 62 (LEU), 80 (PHE). The active sites for 2-Cl-4-NP interacting with 1DLT are: 55 (TYR), 58 (GLY), 59 (VAL), 62 (LEU), 71 (ALA), 74 (LEU), 75 (SER), 78 (LEU), 80 (PHE). The active sites for 2-Cl-6-NP interacting with 1DLT are: 55 (TYR), 58 (GLY), 59 (VAL), 62 (LEU), 65 (LEU), 71 (ALA), 74 (LEU), 75 (SER), 78 (LEU), 80 (PHE). The active sites for 2-Cl-4,6-DNP interacting with 1DLT are: 41 (LEU), 45 (ILE), 50 (ILE), 54 (GLU), 55 (TYR), 58 (GLY), 59 (VAL), 62 (LEU), 80 (PHE). The selected mutation sites were identified from docking-derived residue interaction patterns near the binding pocket. These residues were used as candidate positions for exploratory rational redesign; however, we acknowledge that catalytic performance is also influenced by active-site geometry, substrate orientation, and local electronic environment. The selected mutation sites were identified from docking-derived residue interaction patterns near the binding pocket. These residues were used as candidate positions for exploratory rational redesign; however, we acknowledge that catalytic performance is also influenced by active-site geometry, substrate orientation, and local electronic environment.

3.5.2. Homology Modeling and Model Validation of Novel Dual-Oxygenase with Strong Environmental Adaptability

The amino acid sequences of the 1,2-dihydroxyanisole 1,2-dioxygenase and the six engineered novel dioxygenases (designated 1DLT-1 to 1DLT-6) were determined by querying the NCBI database. Their amino acid sequences are as follows (Figure 5).

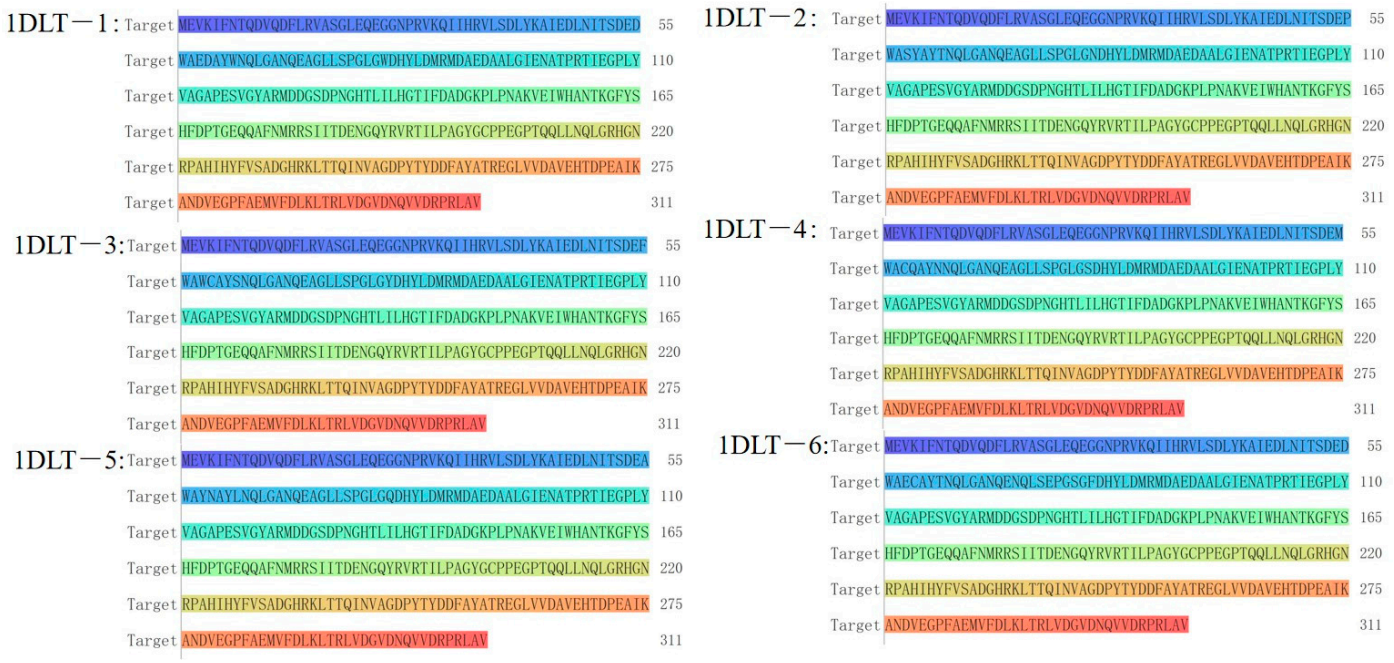

Figure 5. Schematic diagram of dioxygenase and six novel dioxygenase amino acid residues.

The observed homology between the optimized enzyme and the template enzyme exceeded 90%, thereby substantiating the rationality of the selected template enzyme [101]. To further validate the structural validity of the constructed models, the Ramachandran diagram from the UCLA-DOE SAVES server was employed to evaluate the structures of the novel degradative enzymes 1DLT-1 to 1DLT-6. As illustrated in Figure 6, the Ramachandran plot indicates that all structures are located within the optimal region (93.70%, 93.10%, 93.90%, 93.70%, 93.90%, 93.70%) and the semi-permissible region (6.30%, 6.70%, 6.10%, 6.30%, 6.10%, 6.30%), as well as the generally acceptable region (0.00%, 0.20%, 0.00%, 0.00%, 0.00%, 0.00%), collectively accounting for 100%, thereby exceeding the 95% model quality requirement [74].

Subsequently, we performed molecular docking between the modified enzyme and contaminant molecules. The binding energy was calculated using the kinetic method as outlined in Section 2.5. The results of this study are presented in Figure 7. It has been observed that 1DLT-1 exhibits enhanced binding favorability for 2-Cl-4-NP, 2-Cl-6-NP, 2-Cl-4,6-DNP, PNP, 2,6-DNP, and TNP. The 1DLT-6 enzyme exhibited a higher degree of degradation for 2-Cl-4-NP and 2,4-DNP in comparison to the template enzyme. The maximum increase in binding energy (absolute value) observed between the modified enzymes and the template enzyme was 26.997%. In the context of contaminated sites that have undergone pretreatment with the PS-AOP process, the application of enzymatic degradation of NPs has been shown to significantly mitigate adverse effects, including site acidification and SO_4^{2-} residue, resulting from the PS-AOP process. This mitigation is achieved through the combined use of 1DLT-1, 1DLT-6, and 1DLT.

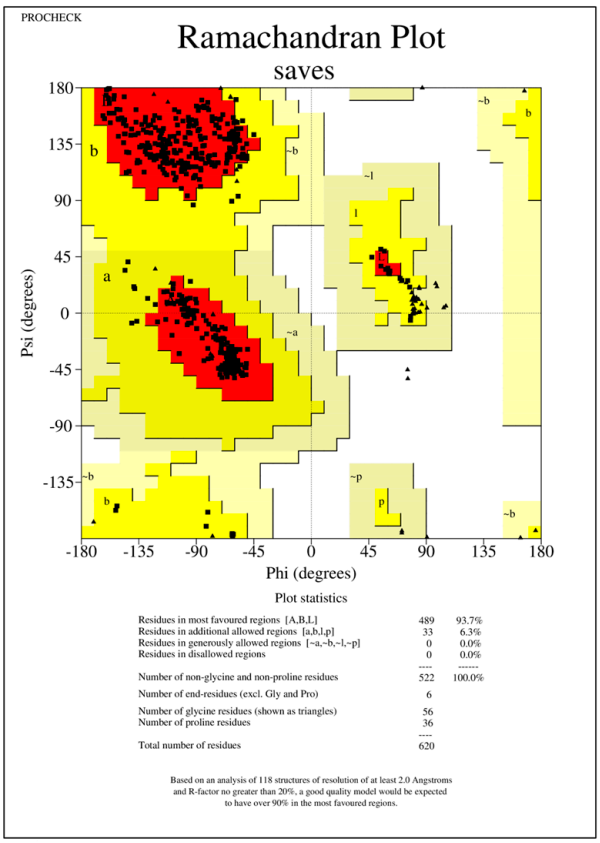

1DLT-1

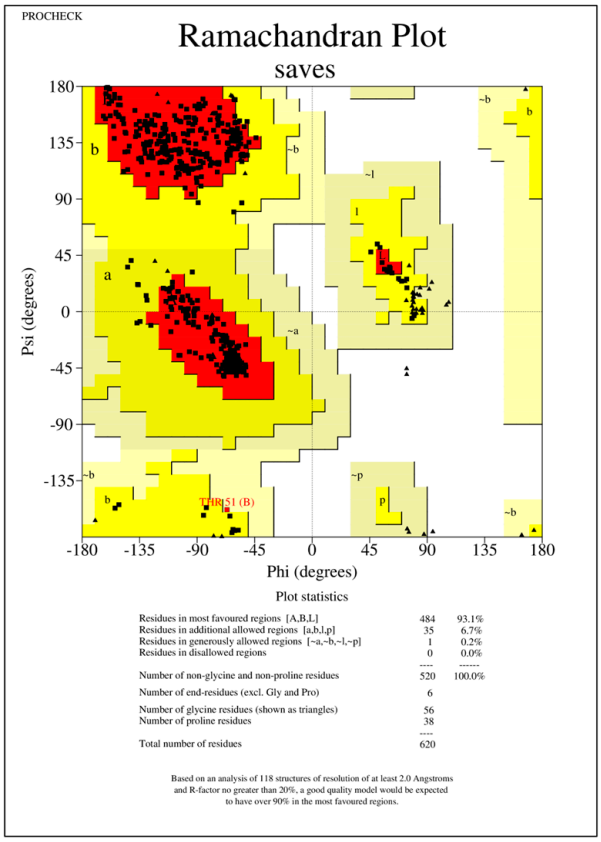

1DLT-2

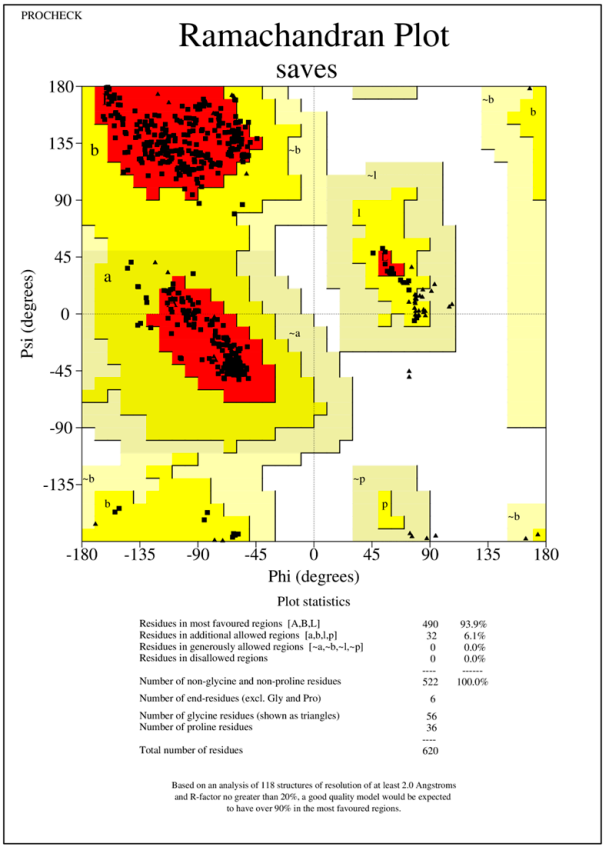

1DLT-3

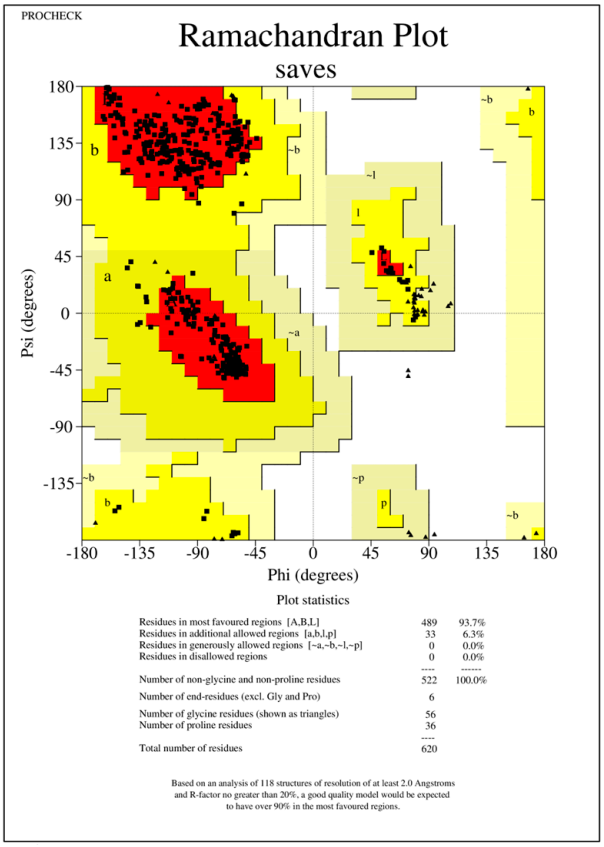

1DLT-4

Figure 6. *Cont.*

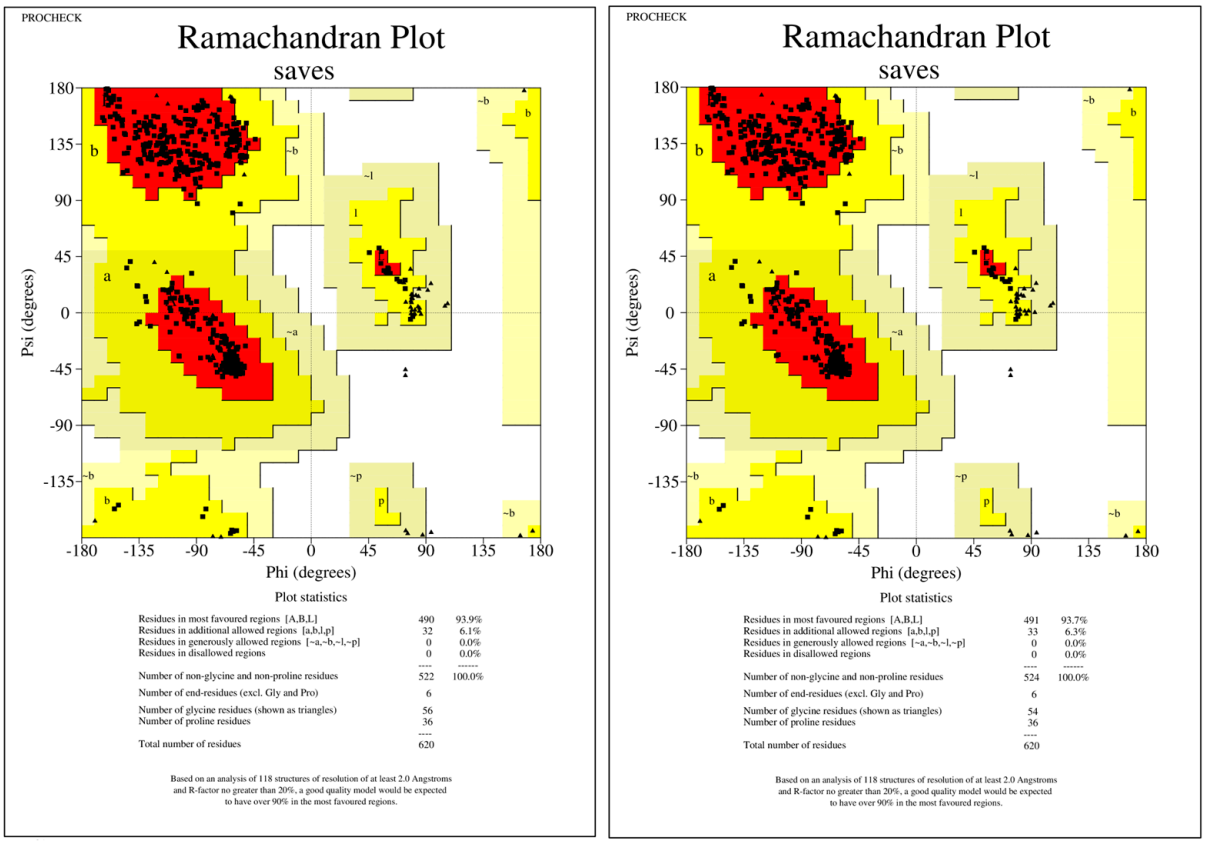

1DLT-5 **1DLT-6**

Figure 6. Ramachandran Conformation Diagram.

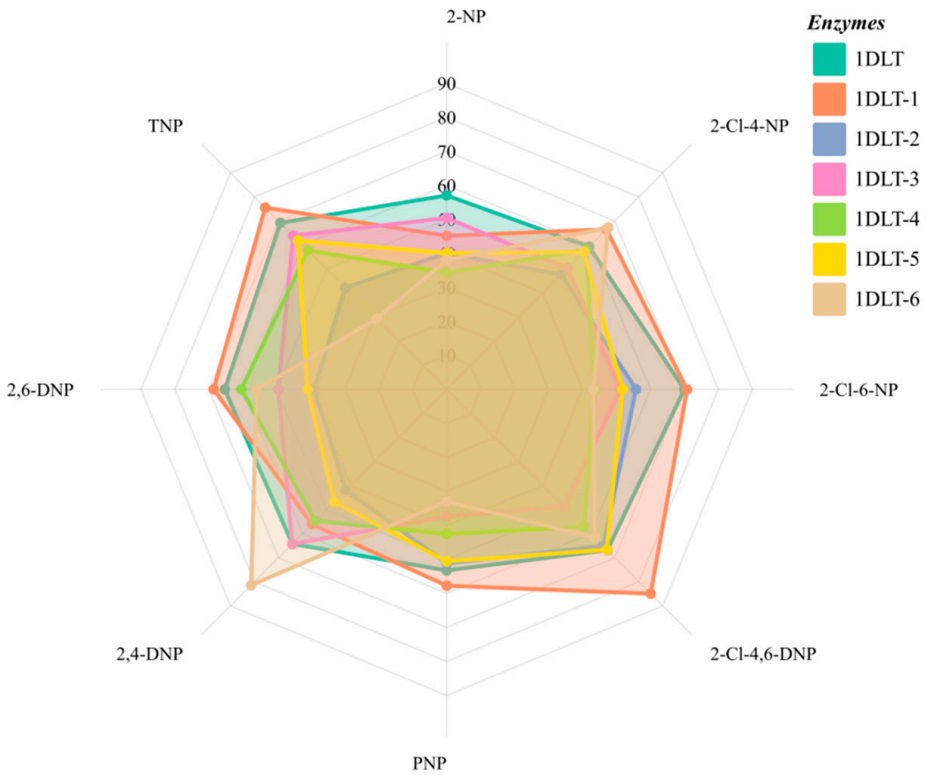

Figure 7. Comparison of binding energies between modified enzymes and template enzymes.

3.6. Mechanism Analysis of Microbial Degradative Enzymes Degrading NPs Based on Molecular Docking

3.6.1. Mechanistic Analysis Based on Amino Acid Residue Interactions Theory

This study analyzes the degradation mechanism of degradation enzymes on NPs based on molecular docking results, utilizing amino acid two-dimensional (2D) surface plots and non-bond interaction diagrams from enzyme–ligand interaction theory. As previously discussed, the newly designed degradation enzymes exhibit distinct degradation patterns for different pollutants. To ensure the validity of the analysis, the selected enzymes exhibit varying degradation efficiencies for the three molecules. Each enzyme exhibits optimal degradation performance for a specific pollutant within the group. Therefore, we selected 1DLT which appears more compatible with 2-NP, 1DLT-6 for its superior degradation of 2-Cl-4-NP, and 1DLT-1 for its most significant improvement in TNP degradation. Subsequent to the docking results between the molecules and their protein receptors, the amino acid residues surrounding the three molecules were analyzed. Amino acid residues interacting with the molecules via van der Waals forces are represented by green circles, while those interacting via electrostatic forces are shown as purple circles [75]. The outcomes of the docking process are demonstrated in Figure 8.

A comparative analysis of molecular docking results between degrading enzymes 1DLT, 1DLT-1, and 1DLT-6 and the pollutant molecule 2-NP was conducted. The results indicated that, in comparison to the amino acid residues surrounding the highly effective degrading protein 1DLT, the proteins with intermediate binding favorability (1DLT-1) and the least effective protein (1DLT-6) exhibited an overall decrease in the total number of amino acid residues interacting via van der Waals forces and electrostatic forces. This finding is consistent with the results presented in Section 3.4, which indicate a positive correlation between lower binding energy and enhanced binding favorability. The pollutant molecule 2-NP interacts with 1DLT enzyme via six amino acid residues through van der Waals forces and four amino acid residues through electrostatic forces, totaling ten residues (Figure 8a). The 1DLT-1 enzyme, which exhibited the second-best binding favorability, had five amino acid residues interacting via van der Waals forces and four via electrostatic forces, totaling nine residues (Figure 8b). The 1DLT-6 enzyme, which exhibited the poorest binding favorability, had five amino acid residues interacting via van der Waals forces and four via electrostatic forces, totaling nine residues (Figure 8c). The observed differences in van der Waals and electrostatic contacts provide a qualitative view of enzyme–ligand interaction patterns, but they should not be interpreted as the sole determinants of catalytic performance. This observation provides a novel perspective for investigating the degradation capacity of enzymes toward 2-NP by examining the properties of van der Waals-interacting amino acids. The pollutant molecule 2-Cl-4-NP has been observed to interact with three amino acid residues surrounding the 1DLT-6 enzyme via van der Waals forces and six residues via electrostatic forces, resulting in a total of nine residues (see Figure 8f). A similar interaction pattern has been observed for the 1DLT-1 enzyme, which is surrounded by three amino acid residues interacting via van der Waals forces and six residues interacting via electrostatic forces, yielding a total of nine residues (see Figure 8e). The 1DLT enzyme has also been observed to be surrounded by three amino acid residues interacting via van der Waals forces and six residues interacting via electrostatic forces, resulting in a total of nine residues (see Figure 8d). As illustrated in Figure 8g–i, the contaminant molecule TNP interacts with nine amino acid residues via van der Waals forces and four amino acid residues via electrostatic forces around the 1DLT-1 enzyme, totaling nine residues. Similarly, three amino acid residues interact with the 1DLT-6 enzyme via van der Waals forces and six via electrostatic forces, also totaling nine. Finally, four amino acid residues interact with the 1DLT enzyme via van der Waals

forces and five via electrostatic forces, also totaling nine. It can be inferred that non-covalent interactions between NPs-like molecules and receptor enzymes are the primary factors influencing the binding capacity of the receptor enzymes (1DLT, 1DLT-1, 1DLT-6).

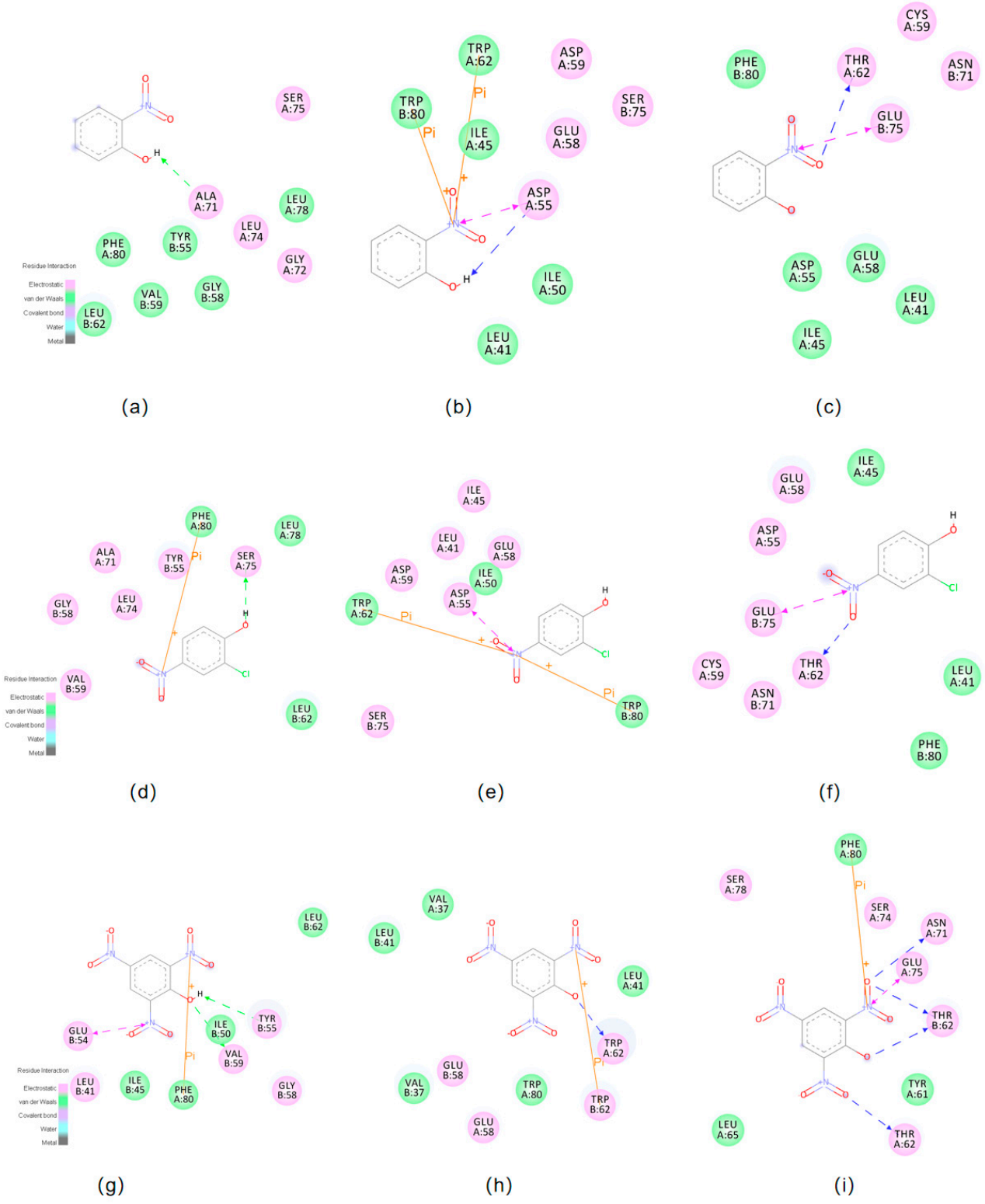

Figure 8. (**a**) 1DLT, (**b**) 1DLT-1, (**c**) Molecular docking results for 1DLT-6 and 2-NP. (**d**) 1DLT, (**e**) 1DLT-1, (**f**) Molecular docking results for 1DLT-6 and 2-Cl-4-NP. (**g**) 1DLT, (**h**) 1DLT-1, (**i**) Molecular docking results for 1DLT-6 and TNP.

3.6.2. Mechanism Analysis of Non-Covalent Interactions Based on Kinetic Simulation

Molecular dynamics methods grounded in Newtonian mechanics have proven effective in simulating the movement and interactions within molecular systems. The GROMACS algorithm facilitates the precise calculation of the energy of intermolecular interactions. This study utilizes GROMACS 5.1.4 software to conduct kinetic simulations of template enzymes (1 MHZ, 3G02, O68978) with secondary pollutants exhibiting high overall toxicity: TNP, 2-Cl-4-NP, and 2-NP. The van der Waals energy, electrostatic energy, polar solvation energy, and nonpolar solvation energy (SASA energy) of the docked complexes are determined by calculations. This quantitative analysis, evaluated from an energy perspective, elucidates the reasons for the differing degradation capabilities of the enzymes (1 MHZ, 3G02, O68978) and quantifies the extent to which different interactions influence the degradation of NPs in groundwater and soil. The calculation formula was

$$\Delta Gb = \Delta EvdW + \Delta Ee + \Delta GPS + \Delta GSASA \quad (7)$$

In Table 5, which utilizes 1DLT, 1DLT-1, and 1DLT-6 as case studies, the results pertaining to van der Waals energy, polar solvation energy, and nonpolar solvation energy for the enzyme-NP complex are presented. During the degradation of 2-NP, the van der Waals energy, polar solvation energy, and nonpolar solvation energy of enzymes 1DLT, 1DLT-1, and 1DLT-6 all increased. Specifically, the van der Waals energy exhibited a range of 18.11% to 32.26%, while the polar solvation energy varied from 111.38% to 158.36%. A decline in electrostatic energy was observed, with variations ranging from 316.79% to 472.16% (absolute value). It is evident that lower values of van der Waals energy, polar solvation energy, and nonpolar solvation energy favor degradation, while higher electrostatic energy promotes degradation. A thorough examination of the range of alterations reveals that electrostatic energy assumes a predominant function in the degradation of 2-NP. During the process of 2-Cl-4-NP degradation, an enhancement in polar solvation energy has been observed to concomitantly increase binding favorability. The rise in electrostatic energy of 1DLT-1 partially influences polar solvation energy changes, thereby explaining the significant disparity in polar solvation energy between the two modified enzymes. Furthermore, during the process of TNP degradation, the modified enzymes demonstrated higher van der Waals energy in comparison to the template enzyme, while exhibiting reduced polar solubilization energy. This finding suggests that van der Waals forces and polar solubilization energy play a substantial role in determining the binding capacity between degradative enzymes and NPs. Of particular interest is the finding that a notable reduction in electrostatic energy had a substantial impact on binding favorability. The binding favorability of the most effective 1DLT-1 exhibited a change rate of 139.93% (absolute value).

Table 5. The effect of different interaction energies between degradative enzymes and NPs.

Compounds	Enzymes	ΔG_b (kJ/mol)	ΔE_{vdW} (kJ/mol)	Percentage Improvement of (ΔE_{vdW}, %)	ΔE_e (kJ/mol)	Percentage Improvement of (ΔE_{vdW}, %)	ΔG_{PS} (kJ/mol)	Percentage Improvement of (ΔE_{vdW}, %)	ΔG_{SASA} (kJ/mol)
2-NP	1DLT	−57.022	−73.261		−14.531		39.927		−9.157
	1DLT-1	−45.150	−59.990	18.11	−60.564	−316.79	84.399	111.38	−8.994
	1DLT-6	−38.038	−49.628	32.26	−83.141	−472.16	103.157	158.36	−8.425
2-Cl-4-NP	1DLT	−59.319	−66.969		−3.734		19.688		−8.304
	1DLT-1	−66.537	−75.363	−12.53	−2.742	26.57	21.276	8.07	−9.709
	1DLT-6	−67.219	−63.124	5.74	−71.568	−1816.66	77.157	291.89	−9.685
TNP	1DLT	−57.491	−90.720		−8.755		52.232		−10.248
	1DLT-1	−75.587	−79.806	12.03	−21.006	−139.93	35.774	−31.51	−10.548
	1DLT-6	−62.526	−71.472	21.22	−2.592	70.39	20.318	−61.10	−8.779

Note: Here, ΔG_b denotes the total binding free energy; ΔE_{vdW}, van der Waals interaction energy; ΔE_e, electrostatic interaction energy; ΔG_{PS}, polar solvation energy; and ΔG_{SASA}, nonpolar solvation energy estimated from solvent-accessible surface area.

The aforementioned analysis lends further credence to the conclusion that higher molecular docking binding energy is associated with enhanced binding efficiency between NPs and enzymes, based on disparities in the magnitude of intermolecular interaction energies.

4. Conclusions

This study proposes a strategy for addressing secondary pollution generated during petroleum hydrocarbon remediation by persulfate-based advanced oxidation processes. DFT calculations using the Gaussian 09 program revealed that conversion pathways for all NPs except 2,6-DNP and 2-Cl-6-NP exhibited values below 0 kJ/mol. The TOPKAT model validated that NPs pose human exposure risks for biological mutagenicity, carcinogenicity, skin irritation, skin sensitization, and eye irritation. A weighted scoring method was employed to identify NPs with high overall toxicity (TNP, 2-Cl-4-NP, 2-NP). Molecular dynamics simulations were utilized to calculate binding energies between pollutant molecules and protein receptors, investigating degradation efficiencies across 27 enzymes. Future work should employ longer MD trajectories together with RMSD/RMSF and convergence analyses to improve the robustness of the energetic evaluation. Among the screened enzymes, catechol 1,2-dioxygenase from Acinetobacter baylyi ADP1 exhibited relatively favorable binding interactions with several high-priority NPs, suggesting that it may be a promising candidate for further mechanistic and experimental evaluation. Given the established fact that residual SO_4^{2-} from PS-AOP treatment at contaminated sites has been shown to impair enzyme activity, the present study has devised a novel approach by modifying amino acid sequences via the use of a technique known as "homology modeling." Enzymes 1DLT-1 and 1DLT-6 exhibited enhanced degradation of all pollutants except 2-NP. The redesigned 1DLT variants should be regarded as computationally proposed candidates for future validation rather than experimentally indicated improved biocatalysts. Finally, molecular docking-based analysis of amino acid residues and non-bonding interaction energies elucidated the degradation mechanism of NPs by the enzyme, supporting the idea that more favorable computed binding interactions may be associated with stronger enzyme–substrate compatibility within the current screening framework, while direct catalytic validation remains necessary. This study contributes to the theoretical research on PS-AOP methods by exploring the feasibility of utilizing microorganisms to address secondary pollution in sodium persulfate advanced oxidation processes. It identifies an enzyme with the best comprehensive degradation performance, designs novel degradative enzymes, and provides theoretical support for microbial degradation of NPs.

Supplementary Materials: The following supporting information can be downloaded at: https://www.mdpi.com/article/10.3390/su18083803/s1 (Supplementary Materials include molecular dynamics simulation code).

Author Contributions: Conceptualization, C.X.; methodology, C.X., Z.R., X.J., J.Y. and Y.L.; software, C.X. and Z.R.; validation, C.X., Z.R., X.J., J.Y. and Y.L.; formal analysis, C.X. and Z.R.; investigation, C.X.; resources, C.X.; data curation, C.X. and Z.R.; writing—original draft preparation, C.X.; writing—review and editing, C.X., Z.R., X.J., J.Y., Y.L., W.F. and S.S.; visualization, C.X., Z.R., X.J., J.Y. and Y.L.; supervision, S.S.; project administration, S.S. All authors have read and agreed to the published version of the manuscript.

Funding: This research received no external funding.

Institutional Review Board Statement: Not applicable.

Informed Consent Statement: Not applicable.

Data Availability Statement: The original contributions presented in this study are included in the article/Supplementary Material. Further inquiries can be directed to the corresponding authors.

Conflicts of Interest: Author Wei Fan is employed by the Baicheng City Yinnen to Baicheng Project Construction Management BurearBureau. The remaining authors declare that the research was conducted in the absence of any commercial or financial relationships that could be construed as a potential conflict of interest.

References

1. Watts, R.J.; Ahmad, M.; Hohner, A.K.; Teel, A.L. Persulfate activation by glucose for in situ chemical oxidation. *Water Res.* **2018**, *133*, 247–254. [CrossRef] [PubMed]
2. Li, Y.; Zhao, L.; Chen, F.; Jin, K.S.; Fallgren, P.H.; Chen, L. Oxidation of nine petroleum hydrocarbon compounds by combined hydrogen peroxide/sodium persulfate catalyzed by siderite. *Environ. Sci. Pollut. Res.* **2020**, *27*, 25655–25663. [CrossRef] [PubMed]
3. Li, S.; Jiang, X.; Xu, W.; Li, M.; Liu, Z.; Han, W.; Yu, C.; Li, J.; Wang, H.; Yeung, K.L. Unveiling electron transfer and radical transformation pathways in coupled electrocatalysis and persulfate oxidation reactions for complex pollutant removal. *Water Res.* **2024**, *267*, 122456. [CrossRef] [PubMed]
4. Anipsitakis, G.P.; Dionysiou, D.D. Degradation of organic contaminants in water with sulfate radicals generated by the conjunction of peroxymonosulfate with cobalt. *Environ. Sci. Technol.* **2003**, *37*, 4790–4797. [CrossRef] [PubMed]
5. Dzengel, J.; Theurich, J.; Bahnemann, D.W. Formation of nitroaromatic compounds in advanced oxidation processes: Photolysis versus photocatalysis. *Environ. Sci. Technol.* **1999**, *33*, 294–300. [CrossRef]
6. Chiron, S.; Minero, C.; Vione, D. Occurrence of 2,4-dichlorophenol and of 2,4-dichloro-6-nitrophenol in the rhône river delta (southern France). *Environ. Sci. Technol.* **2007**, *41*, 3127–3133. [CrossRef]
7. Ji, Y.; Wang, L.; Jiang, M.; Lu, J.; Ferronato, C.; Chovelon, J.-M. The role of nitrite in sulfate radical-based degradation of phenolic compounds: An unexpected nitration process relevant to groundwater remediation by in-situ chemical oxidation (ISCO). *Water Res.* **2017**, *123*, 249–257. [CrossRef] [PubMed]
8. Bedini, A.; Maurino, V.; Minero, C.; Vione, D. Theoretical and experimental evidence of the photonitration pathway of phenol and 4-chlorophenol: A mechanistic study of environmental significance. *Photochem. Photobiol. Sci.* **2012**, *11*, 418–424. [CrossRef]
9. Ji, Y.; Shi, Y.; Yang, Y.; Yang, P.; Wang, L.; Lu, J.; Li, J.; Zhou, L.; Ferronato, C.; Chovelon, J.-M. Rethinking sulfate radical-based oxidation of nitrophenols: Formation of toxic polynitrophenols, nitrated biphenyls and diphenyl ethers. *J. Hazard. Mater.* **2019**, *361*, 152–161. [CrossRef]
10. Potts, A.J.; Bowman, N.J.; Seger, D.L.; Thomas, S.H.L. Toxicoepidemiology and predictors of death in 2,4-dinitrophenol (DNP) toxicity. *Clin. Toxicol.* **2021**, *59*, 515–520. [CrossRef]
11. Wollin, K.-M.; Dieter, H.H. Toxicological guidelines for monocyclic nitro-, amino- and aminonitroaromatics, nitramines, and nitrate esters in drinking water. *Arch. Environ. Contam. Toxicol.* **2005**, *49*, 18–26. [CrossRef] [PubMed]
12. Li, Y.; Cao, Y.; Zhou, X.; Wang, F.; Shan, T.; Li, Z.; Xu, W.; Li, C. Effects of zinc sulfate pretreatment on heat tolerance of bama miniature pig under high ambient temperature1. *J. Anim. Sci.* **2015**, *93*, 3421–3430. [CrossRef] [PubMed]
13. Rudel, R. Predicting health effects of exposures to compounds with estrogenic activity: Methodological issues. *Environ. Health Perspect.* **1997**, *105*, 655–663.
14. Bel Hadjltaief, H.; Sdiri, A.; Ltaief, W.; Da Costa, P.; Gálvez, M.E.; Ben Zina, M. Efficient removal of cadmium and 2-chlorophenol in aqueous systems by natural clay: Adsorption and photo-fenton degradation processes. *Comptes Rendus Chim.* **2017**, *21*, 253–262. [CrossRef]
15. Arora, P.; Sharma, A.; Mehta, R.; Shenoy, B.; Srivastava, A.; Singh, V. Metabolism of 4-chloro-2-nitrophenol in a gram-positive bacterium, *Exiguobacterium* sp. PMA. *Microb. Cell Factories* **2012**, *11*, 150. [CrossRef] [PubMed]
16. Arora, P.K.; Bae, H. Biotransformation and chemotaxis of 4-chloro-2-nitrophenol by *Pseudomonas* sp. JHN. *Microb. Cell Factories* **2014**, *13*, 110. [CrossRef] [PubMed]
17. Guo, Y.; Li, D.-F.; Zheng, J.; Xu, Y.; Zhou, N.-Y. Single-Component and Two-Component para-Nitrophenol Monooxygenases: Structural Basis for Their Catalytic Difference. *Appl. Environ. Microbiol.* **2021**, *87*, e0117121. [CrossRef]
18. Ke, Z.; Lan, M.; Yang, T.; Jia, W.; Gou, Z.; Chen, K.; Jiang, J. A two-component monooxygenase for continuous denitration and dechlorination of chlorinated 4-nitrophenol in *Ensifer* sp. strain 22-1. *Environ. Res.* **2021**, *198*, 111216. [CrossRef]
19. Zhang, J.-J.; Liu, H.; Xiao, Y.; Zhang, X.-E.; Zhou, N.-Y. Identification and characterization of catabolic *para* -nitrophenol 4-monooxygenase and *para* -benzoquinone reductase from *Pseudomonas* sp. Strain WBC-3. *J. Bacteriol.* **2009**, *191*, 2703–2710. [CrossRef]
20. Pakala, S.B.; Gorla, P.; Pinjari, A.B.; Krovidi, R.K.; Baru, R.; Yanamandra, M.; Merrick, M.; Siddavattam, D. Biodegradation of methyl parathion and p-nitrophenol: Evidence for the presence of a p-nitrophenol 2-hydroxylase in a gram-negative *Serratia* sp. strain DS001. *Appl. Microbiol. Biotechnol.* **2007**, *73*, 1452–1462. [CrossRef]

21. Kollock, R.; Rost, K.; Batke, M.; Glatt, H. Effect of pentachlorophenol and 2,6-dichloro-4-nitrophenol on the activity of cDNA-expressed human alcohol and aldehyde dehydrogenases. *Toxicol. Lett.* **2009**, *191*, 360–364. [CrossRef]
22. Ro, S.Y.; Ross, M.O.; Deng, Y.W.; Batelu, S.; Lawton, T.J.; Hurley, J.D.; Stemmler, T.L.; Hoffman, B.M.; Rosenzweig, A.C. From micelles to bicelles: Effect of the membrane on particulate methane monooxygenase activity. *J. Biol. Chem.* **2018**, *293*, 10457–10465. [CrossRef]
23. Vikram, S.; Pandey, J.; Bhalla, N.; Pandey, G.; Ghosh, A.; Khan, F.; Jain, R.K.; Raghava, G.P. Branching of the p-nitrophenol (PNP) degradation pathway in *Burkholderia* sp. Strain SJ98: Evidences from genetic characterization of PNP gene cluster. *AMB Express* **2012**, *2*, 30. [CrossRef] [PubMed]
24. Jensen, C.N.; Ali, S.T.; Allen, M.J.; Grogan, G. Exploring nicotinamide cofactor promiscuity in NAD(P)H-dependent flavin containing monooxygenases (FMOs) using natural variation within the phosphate binding loop. Structure and activity of FMOs from *Cellvibrio* sp. BR and *Pseudomonas stutzeri* NF13. *J. Mol. Catal. B Enzym.* **2014**, *109*, 191–198. [CrossRef] [PubMed]
25. Leung, K.T.; Campbell, S.; Gan, Y.; White, D.C.; Lee, H.; Trevors, J.T. The role of the *Sphingomonas* species UG30 pentachlorophenol-4-monooxygenase in p-nitrophenol degradation. *FEMS Microbiol. Lett.* **1999**, *173*, 247–253. [CrossRef]
26. Webb, B.N.; Ballinger, J.W.; Kim, E.; Belchik, S.M.; Lam, K.-S.; Youn, B.; Nissen, M.S.; Xun, L.; Kang, C. Characterization of chlorophenol 4-monooxygenase (TftD) and NADH:FAD oxidoreductase (TftC) of *Burkholderia cepacia* AC1100. *J. Biol. Chem.* **2010**, *285*, 2014–2027. [CrossRef]
27. Xu, L.-H.; Fushinobu, S.; Ikeda, H.; Wakagi, T.; Shoun, H. Crystal structures of cytochrome P450 105P1 from *Streptomyces avermitilis*: Conformational flexibility and histidine ligation state. *J. Bacteriol.* **2009**, *191*, 1211–1219. [CrossRef] [PubMed]
28. Haigler, B.E.; Suen, W.C.; Spain, J.C. Purification and sequence analysis of 4-methyl-5-nitrocatechol oxygenase from *Burkholderia* sp. strain DNT. *J. Bacteriol.* **1996**, *178*, 6019–6024. [CrossRef]
29. Li, L.; Liu, X.; Yang, W.; Xu, F.; Wang, W.; Feng, L.; Bartlam, M.; Wang, L.; Rao, Z. Crystal structure of long-chain alkane monooxygenase (LadA) in complex with coenzyme FMN: Unveiling the long-chain alkane hydroxylase. *J. Mol. Biol.* **2008**, *376*, 453–465. [CrossRef] [PubMed]
30. Whittington, D.A.; Rosenzweig, A.C.; Frederick, C.A.; Lippard, S.J. Xenon and halogenated alkanes track putative substrate binding cavities in the soluble methane monooxygenase hydroxylase. *Biochemistry* **2001**, *40*, 3476–3482. [CrossRef]
31. Kim, H.; An, S.; Park, Y.R.; Jang, H.; Yoo, H.; Park, S.H.; Lee, S.J.; Cho, U.-S. MMOD-induced structural changes of hydroxylase in soluble methane monooxygenase. *Sci. Adv.* **2019**, *5*, eaax0059. [CrossRef] [PubMed]
32. Tully, B.J.; Graham, E.D.; Heidelberg, J.F. The reconstruction of 2,631 draft metagenome-assembled genomes from the global oceans. *Sci. Data* **2018**, *5*, 170203. [CrossRef]
33. Elango, N.A.; Radhakrishnan, R.; Froland, W.A.; Wallar, B.J.; Earhart, C.A.; Lipscomb, J.D.; Ohlendorf, D.H. Crystal structure of the hydroxylase component of methane monooxygenase from *Methylosinus trichosporium* OB3b: Structure methane monooxygenase hydroxylase. *Protein Sci.* **1997**, *6*, 556–568. [CrossRef]
34. Jones, J.C.; Banerjee, R.; Shi, K.; Aihara, H.; Lipscomb, J.D. Structural studies of the *Methylosinus trichosporium* OB3b soluble methane monooxygenase hydroxylase and regulatory component complex reveal a transient substrate tunnel. *Biochemistry* **2020**, *59*, 2946–2961. [CrossRef]
35. Díaz-Sánchez, Á.G.; González-Segura, L.; Mújica-Jiménez, C.; Rudiño-Piñera, E.; Montiel, C.; Martínez-Castilla, L.P.; Muñoz-Clares, R.A. Amino acid residues critical for the specificity for betaine aldehyde of the plant ALDH10 isoenzyme involved in the synthesis of glycine betaine. *Plant Physiol.* **2012**, *158*, 1570–1582. [CrossRef]
36. Tao, X.; Zhang, Z.; Zhang, X.; Li, H.; Sun, H.; Mao, Z.-W.; Xia, W. Structural Insight into the Substrate Gating Mechanism by *Staphylococcus aureus* Aldehyde Dehydrogenase. *CCS Chem.* **2020**, *2*, 946–954. [CrossRef]
37. Valencia, E.; Larroy, C.; Ochoa, W.F.; Parés, X.; Fita, I.; Biosca, J.A. Apo and holo structures of an NADP(H)-dependent cinnamyl alcohol dehydrogenase from *Saccharomyces cerevisiae*. *J. Mol. Biol.* **2004**, *341*, 1049–1062. [CrossRef]
38. Kovaleva, E.G.; Lipscomb, J.D. Crystal structures of Fe^{2+} dioxygenase superoxo, alkylperoxo, and bound product intermediates. *Science* **2007**, *316*, 453–457. [CrossRef] [PubMed]
39. Ramdass, A.C.; Rampersad, S.N. Draft genome of hydrocarbon-degrader *Burkholderia cepacia* BCTT, isolated from soil chronically polluted with crude oil in trinidad. *Microbiol. Resour. Announc.* **2024**, *13*, e00902-24. [CrossRef] [PubMed]
40. Vetting, M.W.; Ohlendorf, D.H. The 1.8 Å crystal structure of catechol 1,2-dioxygenase reveals a novel hydrophobic helical zipper as a subunit linker. *Structure* **2000**, *8*, 429–440. [CrossRef] [PubMed]
41. Earhart, C.A.; Vetting, M.W.; Gosu, R.; Michaud-Soret, I.; Que, L.; Ohlendorf, D.H. Structure of catechol 1,2-dioxygenase from *Pseudomonas arvilla*. *Biochem. Biophys. Res. Commun.* **2005**, *338*, 198–205. [CrossRef]
42. Moon, J.; Kang, E.; Min, K.R.; Kim, C.K.; Min, K.H.; Lee, K.S.; Kim, Y. Characterization of the gene encoding catechol 2,3-dioxygenase from *Achromobacter xylosoxidans* KF701. *Biochem. Biophys. Res. Commun.* **1997**, *238*, 430–435. [CrossRef]
43. Cho, J.-H.; Jung, D.-K.; Lee, K.; Rhee, S. Crystal structure and functional analysis of the extradiol dioxygenase LapB from a long-chain alkylphenol degradation pathway in *Pseudomonas*. *J. Biol. Chem.* **2009**, *284*, 34321–34330. [CrossRef]

44. Micalella, C.; Martignon, S.; Bruno, S.; Pioselli, B.; Caglio, R.; Valetti, F.; Pessione, E.; Giunta, C.; Rizzi, M. X-ray crystallography, mass spectrometry and single crystal microspectrophotometry: A multidisciplinary characterization of catechol 1,2 dioxygenase. *Biochim. Biophys. Acta* **2011**, *1814*, 817–823. [CrossRef] [PubMed]
45. Reetz, M.T.; Bocola, M.; Wang, L.-W.; Sanchis, J.; Cronin, A.; Arand, M.; Zou, J.; Archelas, A.; Bottalla, A.-L.; Naworyta, A.; et al. Directed evolution of an enantioselective epoxide hydrolase: Uncovering the source of enantioselectivity at each evolutionary stage. *J. Am. Chem. Soc.* **2009**, *131*, 7334–7343. [CrossRef] [PubMed]
46. Sun, Z.; Lonsdale, R.; Kong, X.; Xu, J.; Zhou, J.; Reetz, M.T. Reshaping an enzyme binding pocket for enhanced and inverted stereoselectivity: Use of smallest amino acid alphabets in directed evolution. *Angew. Chem. Int. Ed.* **2015**, *54*, 12410–12415. [CrossRef] [PubMed]
47. Kong, X.-D.; Yuan, S.; Li, L.; Chen, S.; Xu, J.-H.; Zhou, J. Engineering of an epoxide hydrolase for efficient bioresolution of bulky pharmaco substrates. *Proc. Natl. Acad. Sci. USA* **2014**, *111*, 15717–15722. [CrossRef]
48. Mazurek, A.H.; Szeleszczuk, Ł.; Pisklak, D.M. Periodic DFT calculations—Review of applications in the pharmaceutical sciences. *Pharmaceutics* **2020**, *12*, 415. [CrossRef]
49. Peng, X.-L.; Jiang, R.; Jia, C.-S.; Zhang, L.-H.; Zhao, Y.-L. Gibbs free energy of gaseous phosphorus dimer. *Chem. Eng. Sci.* **2018**, *190*, 122–125. [CrossRef]
50. Colmenero, F.; Fernández, A.M.; Cobos, J.; Timón, V. Temperature-dependent gibbs free energies of reaction of uranyl-containing materials based on density functional theory. *J. Phys. Chem. C* **2018**, *122*, 5268–5279. [CrossRef]
51. Ikwu, F.A.; Shallangwa, G.A.; Mamza, P.A. QSAR, QSTR, and molecular docking studies of the anti-proliferative activity of phenylpiperazine derivatives against DU145 prostate cancer cell lines. *Beni-Suef Univ. J. Basic Appl. Sci.* **2020**, *9*, 35. [CrossRef]
52. Taillebois, E.; Cartereau, A.; Jones, A.K.; Thany, S.H. Neonicotinoid insecticides mode of action on insect nicotinic acetylcholine receptors using binding studies. *Pestic. Biochem. Physiol.* **2018**, *151*, 59–66. [CrossRef]
53. Marlatt, V.L.; Leung, T.Y.G.; Calbick, S.; Metcalfe, C.; Kennedy, C. Sub-lethal effects of a neonicotinoid, clothianidin, on wild early life stage sockeye salmon (*Oncorhynchus nerka*). *Aquat. Toxicol.* **2019**, *217*, 105335. [CrossRef] [PubMed]
54. Chavan, B.B.; Tiwari, S.; G, S.; Nimbalkar, R.D.; Garg, P.; R, S.; Talluri, M.V.N.K. In vitro and in vivo metabolic investigation of the palbociclib by UHPLC-Q-TOF/MS/MS and in silico toxicity studies of its metabolites. *J. Pharm. Biomed. Anal.* **2018**, *157*, 59–74. [CrossRef] [PubMed]
55. Hadni, H.; Elhallaoui, M. 2D and 3D-QSAR, molecular docking and ADMET properties in silico studies of azaaurones as antimalarial agents. *New J. Chem.* **2020**, *44*, 6553–6565. [CrossRef]
56. Wang, J.; Dayem Ullah, A.Z.; Chelala, C. IW-scoring: An integrative weighted scoring framework for annotating and prioritizing genetic variations in the noncoding genome. *Nucleic Acids Res.* **2018**, *46*, e47. [CrossRef]
57. Wang, C.; Yang, H.; Pu, Q.; Li, Y. Calculating protein–ligand binding affinities with MMPBSA: Method and error analysis. *J. Comput. Chem.* **2016**, *37*, 2436–2446. [CrossRef]
58. He, W.; Yang, H.; Pu, Q.; Li, Y. Novel control strategies for the endocrine-disrupting effect of PAEs to pregnant women in traffic system. *Sci. Total Environ.* **2022**, *851*, 158269. [CrossRef]
59. Yang, J.; Li, X.; Yang, H.; Zhao, W.; Li, Y. OPFRs in e-waste sites: Integrating in silico approaches, selective bioremediation, and health risk management of residents surrounding. *J. Hazard. Mater.* **2022**, *429*, 128304. [CrossRef]
60. Li, M.; He, W.; Li, Y. Enhanced plant-microbe remediation of PCBs in soil using enzyme modification technique combined with molecular docking and molecular dynamics. *Biochem. J.* **2021**, *478*, 1921–1941. [CrossRef]
61. Wu, F.; Wang, Z.; Li, X.; Wang, X. Amide herbicides: Analysis of their environmental fate, combined plant–microorganism soil remediation scheme, and risk prevention and control strategies for sensitive populations. *J. Hazard. Mater.* **2023**, *460*, 132452. [CrossRef]
62. Seto, W.-K.; Lai, C.-L.; Ip, P.P.C.; Fung, J.; Wong, D.K.-H.; Yuen, J.C.-H.; Hung, I.F.-N.; Yuen, M.-F. A large population histology study showing the lack of association between ALT elevation and significant fibrosis in chronic hepatitis B. *PLoS ONE* **2012**, *7*, e32622. [CrossRef]
63. Ju, K.-S.; Parales, R.E. Nitroaromatic compounds, from synthesis to biodegradation. *Microbiol. Mol. Biol. Rev.* **2010**, *74*, 250–272. [CrossRef]
64. Lam, S.H.; Ung, C.Y.; Hlaing, M.M.; Hu, J.; Li, Z.-H.; Mathavan, S.; Gong, Z. Molecular insights into 4-nitrophenol-induced hepatotoxicity in zebrafish: Transcriptomic, histological and targeted gene expression analyses. *Biochim. Biophys. Acta BBA—Gen. Subj.* **2013**, *1830*, 4778–4789. [CrossRef]
65. Huang, Q.; Wang, L.; Han, S. The genotoxicity of substituted nitrobenzenes and the quantitative structure-activity relationship studies. *Chemosphere* **1995**, *30*, 915–923. [CrossRef]
66. Xu, H.; Zhang, X.; Li, H.; Li, C.; Huo, X.-J.; Hou, L.-P.; Gong, Z. Immune response induced by major environmental pollutants through altering neutrophils in zebrafish larvae. *Aquat. Toxicol.* **2018**, *201*, 99–108. [CrossRef]
67. Han, L.; Chen, S.; Zhou, J. Expression and cloning of *catA* encoding a catechol 1,2-dioxygenase from the 2,4-D-degrading strain *Cupriavidus campinensis* BJ71. *Prep. Biochem. Biotechnol.* **2020**, *50*, 486–493. [CrossRef] [PubMed]

68. Kobayashi, M.; Yamamoto, M. Nrf2–Keap1 regulation of cellular defense mechanisms against electrophiles and reactive oxygen species. *Adv. Enzyme Regul.* **2006**, *46*, 113–140. [CrossRef] [PubMed]
69. Zhang, D.D. Mechanistic studies of the Nrf2-Keap1 signaling pathway. *Drug Metab. Rev.* **2006**, *38*, 769–789. [CrossRef] [PubMed]
70. Preussmann, R. Carcinogenic N-nitroso compounds and their environmental significance. *Naturwissenschaften* **1984**, *71*, 25–30. [CrossRef]
71. Phale, P.S.; Malhotra, H.; Shah, B.A. Degradation strategies and associated regulatory mechanisms/features for aromatic compound metabolism in bacteria. *Adv. Appl. Microbiol.* **2020**, *112*, 1–65. [PubMed]
72. Long, Y.; Yang, S.; Xie, Z.; Cheng, L. Cloning, expression, and characterization of catechol 1,2-dioxygenase from a phenol-degrading *Candida tropicalis* JH8 strain. *Prep. Biochem. Biotechnol.* **2016**, *46*, 673–678. [CrossRef] [PubMed]
73. Guzik, U.; Hupert-Kocurek, K.; Sałek, K.; Wojcieszyńska, D. Influence of metal ions on bioremediation activity of protocatechuate 3,4-dioxygenase from *Stenotrophomonas maltophilia* KB2. *World J. Microbiol. Biotechnol.* **2013**, *29*, 267–273. [CrossRef]
74. Jiang, L.; Li, Y. Modification of PBDEs (BDE-15, BDE-47, BDE-85 and BDE-126) biological toxicity, bio-concentration, persistence and atmospheric long-range transport potential based on the pharmacophore modeling assistant with the full factor experimental design. *J. Hazard. Mater.* **2016**, *307*, 202–212. [CrossRef] [PubMed]
75. Xiao, J.; Zhang, W.; Zhang, S.; Li, Y. Molecular modification of benzophenone derivatives for lower bioenrichment and toxicity through the pharmacophore model. *Chem. Res. Chin. Univ.* **2022**, *38*, 535–545. [CrossRef]